STRUCTURED CONTROL LAWS FOR FLEXIBLE WING CONCEPTS

Filip Svoboda

Doctoral Thesis

STRUCTURED CONTROL LAWS FOR FLEXIBLE WING CONCEPTS

Filip Svoboda

Prague, 2023

Czech Technical University in Prague
Faculty of Electrical Engineering
Department of Control Engineering

Ph.D. Program:
Electrical Engineering and Information Technology

Branch of study:
Control Engineering and Robotics

Supervisor:
Martin Hromčík

Filip Svoboda: *Structured control laws for flexible wing concepts*, Ph.D. thesis, Czech Technical University in Prague, Faculty of Electrical Engineering, 2023

Declaration

This doctoral thesis is submitted in partial fulfillment of the requirements for the degree of doctor (Ph.D.) The work submitted in this thesis is the result of my own investigation, except where otherwise stated. I declare that I worked out this thesis independently and I quoted all used sources of information in accord with Methodical instructions of CTU in Prague about ethical principles for writing academic thesis. Moreover I declare that it has not already been accepted for any degree and is also not being concurrently submitted for any other degree.

In Prague, 2023

.....

Filip Svoboda

Abstract

Developments in the field of aviation have been constantly pushing the boundaries of aircraft in terms of dynamics, performance, and efficiency. Concepts which were previously only theoretical, are now becoming feasible thanks to new materials, actuators, control systems, and other technologies. Wings are becoming lighter, more efficient, and more flexible with composite materials and new designs. This brings new challenges in terms of control and safety. In parallel, new concepts such as morphing wings, are replacing conventional control surfaces with a smooth and deformable wing, which deforms in a controlled manner and thereby ensures the function of the control surfaces. This work deals with the design of structured control laws motivated by developments in flexible and morphing wings. The dynamics of these systems tend to be quite complex. However, we can recognize specific structures and identify links within the system to guide the control design. With an appropriate interpretation of the model and the mentioned links, control design can be approached in a structured way. The advantages of such approach are the distribution of the task into smaller and more manageable units, easy scaling, and intuitive tuning. The design of decentralized control laws based on the system's structure is firstly presented on a one-dimensional structure in Chapter 2. However, the mentioned approach cannot be directly applied to multidimensional systems which are the main motivation of this work. Therefore, a second algorithm for the control law synthesis is proposed in Chapter 3. Even in this case, the task is simplified, but it already uses LMIs and other principles, which are expanded in the fourth chapter, where the controlled system is a wing model represented by a FEM structure together with a model of actuators and aerodynamics.

Keywords: decentralized control, morphing wing, aeroelasticity, active damping, vibration suppression, mechanical structures, linear matrix inequalities

Abstrakt

Vývoj v oblasti letectví neustále posouvá hranice letadel z pohledu dynamiky, výkonu i účinnosti. Dříve pouze teoretické koncepty se stávají realizovatelnými díky novým materiálům, aktuátorům, řídicím systémům a dalším technologiím. Křídla se s kompozitními materiály a novými konstrukcemi stávají lehčí, efektivnější a flexibilnější. To přináší nové výzvy z pohledu řízení a bezpečnosti. Paralelně také vznikají nové koncepty, jako jsou morfující křídla nahrazující konvenční řídicí plochy hladkou a spojitou plochou křídla, které se kontrolovaně deformuje a tím zajišťuje funkce řídicích ploch. Tato práce se zabývá návrhem strukturovaných řídicích zákonů motivovaných flexibilními a morfujícími křídly. Dynamika těchto systémů bývá poměrně komplexní, nicméně v ní můžeme nalézt určité struktury a vazby. Vhodnou interpretací modelu a zmiňovaných vazeb pak lze i k řízení přistoupit strukturovaně. Výhodou je rozložení úlohy na menší a snáze řešitelné celky, snadné škálování a intuitivní ladění. Design decentralizovaných řídicích zákonů, které vychází ze struktury systému, práce prezentuje nejprve na jedno-dimenzionální struktuře. Uvedený přístup ovšem nelze přímo aplikovat na vícedimenzionální systémy, kterými je tato práce motivována. Dále je proto navržen druhý algoritmus pro syntézu řídicího zákonu. I v tomto případě je úloha zjednodušena, nicméně již využívá LMI a další principy, které jsou rozšířeny ve čtvrté kapitole, kde je řízený systém model křídla reprezentovaný FEM strukturou doplněnou o model aktuátorů a aerodynamiky.

Klíčová slova: decentralizované řízení, morfující křídlo, aeroelasticita, aktivní tlumení, potlačení vibrací, mechanické struktury, lineární maticové nerovnosti

Acknowledgements

I would like to express my gratitude to *Martin Hromčík* for sharing his valuable experience, his guidance and support. I also really appreciate an invaluable opportunity to collaborate with Martin on exciting projects for companies like Porsche Engineering, Eaton, or Honeywell. Learning from such an optimistic person was a joy and fun.

My thanks also go to other colleagues and friends from the Department of Control Engineering and Faculty of Mechanical Engineering: *Petr Hušek, Kristian Hengster-Movric, Zdeněk Hurák, Jiří Zemánek, Martin Gurtner, Filip Richter, Krištof Pučejdl, Tomáš Čenský, Zbyněk Šika* and many others. It is a pleasure to be surrounded by such amazing people.

Finally, I want to thank my family, my supportive parents... I am so sorry you can't see it anymore Daddy. You give me power from heaven. My thanks also belong to my grandpa, *Ladislav Svoboda*. He is an incredible support for me! Indescribable gratitude goes to my love *Katka*. Her patience, support, and joy from my successes helped me overcome obstacles.

Contents

1. Introduction

Aircraft wings are the most essential components determining aircraft performance and efficiency. Therefore, considerable effort is focused on weight reduction, increasing wing aspect ratios, wing surface and geometry improvement, etc. These goals also bring requirements on materials and construction. Modern composite materials make it possible to fulfill most requirements very well. The result is then a highly efficient and flexible wing structure where aeroelasticity and loads must be consistently taken into account. Aerodynamics, inertia and elastic forces acting in aeroelastic systems bring aeroelastic phenomena *Flutter* and *Buffetting*. Flutter is the most important of those phenomena, causing a dynamic instability of aeroelastic structures such as wings. It can take various forms involving various interacting modes (wing bending & torsion, wing torsion & control surface, etc). These self-excited oscillations occur above the critical/flutter speed, which can lead to aircraft destruction in a matter of seconds.

Aeroelasticity is thus a required and important part of safety-check procedures during aircraft designs, which all aircraft have to meet. In Europe, civil aircraft are designed to meet *European Union Aviation Safety Agency (EASA)* regulations and standardization. Similar authority in the U.S. is *Federal Aviation Administration (FAA)*. One of their common objectives is ensuring that the aircraft is free from flutter throughout its flight envelope. A minimum required flutter margin is usually 15% above *design dive speed* V_D. That should provide a reasonable safety margin for different mass distributions, variations of structural properties, parameter inaccuracies, etc.

In general, there are two ways to prevent flutter. One way is wing construction redesign respecting the flight envelope and flutter margins. Then, the typical consequence is a weight increase and, thus, an efficiency decrease at the same time. In the second case, the control systems solve this problem

without changing the wing structure. Wing oscillations are suppressed thanks to the appropriate control surface actions based on real-time measurements. The control law thus ensures sufficient damping of the wing. There are many control design strategies used for this purpose.

Goals

We aim to design structured control laws suitable for flexible wing concepts. The control law design respecting the system structure should be easily scalable with clear physical interpretation. Its application must ensure safe and efficient wing function. The dissertation goal could be summarized in the following objectives.

a) Develop easily scalable design algorithms for decentralized control laws focused on active damping of mechanical flexible structures.

b) Expand the developed algorithms to aeroelastic problems, namely to active control approaches for flutter resistance augmentation.

c) Demonstrate applicability of the developed methods for emerging morphing wing concepts.

Outline

This dissertation started with Fixed-Structure H_∞ control synthesis and other approaches applied to the aeroelasticity problems. In this context, we used standard simulation models (based on strip theory) and built a wind tunnel experimental setup (Figure 1.1). Concerning the size of the wind tunnel test section (750mm), the experimental setup was simplified. The rigid wing construction with two control surfaces was mounted on vertical rails with springs

representing wing stiffness and damping. The first control surface represents another degree of freedom coupled with springs. The second control surface was controlled based on information from the accelerometer and dampened the wing.

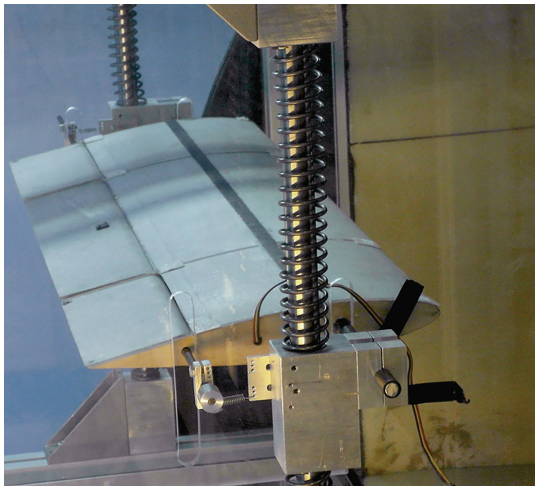

Figure 1.1: Wind tunnel experiment for active flutter attenuation.

The Fixed-Structured H_∞ design methodology offers an efficient method to obtain multivariable control laws with predefined controller structure by specifying closed-loop frequency response requirements. The control design principle is similar to standard H_∞ synthesis. However, we minimize the H_∞ norm under the controller complexity constraints. Thus, we can get low-order controllers even for high-order systems and often without losing much performance compared to full-order design. Fixed-structure H_∞ design also enables consideration of variability in system parameters, which is important from a robustness point of view. The resulting robust controller fulfills its role even under the assumption of expected changes in the system. It could be a

change in mass, altitude, speed, etc.

This approach significantly increases the flutter speed and improves the dynamic behavior of a flexible wing. Nevertheless, the controller tuning realized through the weighting filters does not have to be simple in some cases. Weighting filter design requires a certain experience, and small filter changes may produce dramatically different results.

In 2017 *FlexSys* and *NASA* with *Air Force* successfully flight-tested a *Glufstream III* aircraft with variable geometry trailing edge structure. This experiment made *morphing wings* a realistic solution and variable wing geometry was no longer just science fiction. FlexSys presented a unique *Adaptive Compliant Trailing Edge (ACTE)* with possible deformation from -9° to +40° and a response rate of 30°/s. Then, the direction of the dissertation began to move to the morphing wing control. A morphing wing presents an opportunity to increase the performance and efficiency of an aircraft. However, its control is challenging; nevertheless, completely new control options arise.

Current conventional wings are usually designed for either a single cruise flight condition or by using a weighted combination of multiple flight conditions, and they are thus not optimal for a wide range of flight modes. Continuously variable profile geometries promise significantly increased efficiency, minimized drag, and low noise levels compared to wings with conventional control surfaces with necessary constructional gaps. Morphing wing replaces these control surfaces, such as ailerons, flaps, slats, etc., with a smooth variable changing wing shape.

The ability to smoothly shape a wing profile is associated with special constructions, flexible composite materials, and *smart materials* such as *Shape Memory Alloys (SMA)*. The mechanical construction of morphing wings is still challenging. However, in this area, we can see progress and the efforts of even large institutions and companies such as *NASA* or *Boeing*. Many aca-

demic small-scale projects are also solving questions regarding this topic. We also have developed our constructions (see Figure 1.2) to be able to realize wind tunnel experiments (Figure 1.3) with the morphing wing.

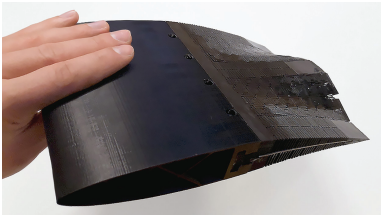

Figure 1.2: Construction of the morphing wing wind tunnel segment.

Our own morphing wing construction is made from a 3D-printed skeleton with flexible patterns in cross-section. The skeleton is flexible and pressure-resistant. Several versions of these constructions were equipped by *Micro Fiber Composite (MFC)*. This actuator type proved inadequate, and the next versions are instrumented with classical servo motors. Servo motors offer more force, and they are also easy to control. A thin layer of latex is glued on the flexible trailing edge construction. It provides sufficient flexibility and covering. The leading edge hides the servos and is covered with stretched foil.

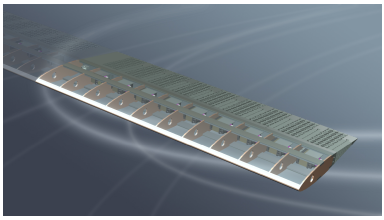

(a) CAD model.

(b) Realization in a wind tunnel.

Figure 1.3: Morphing wing demonstrator.

From the previous description of the morphing wing demonstrator, we can see the wing as a flexible structure with individually controlled fragments containing actuators. The thesis represents this system by a dynamical model combining *FEM* model of the structure, actuators models, and aerodynamics. Details about the model are given later. However, the repetitive structure obtained from FEM modeling and an even distribution of actuators are important. In other words, our dynamical model can be formulated as a set of system fragments connected by physical links inside the dynamical model, see Figure 1.4. Each system fragment contains its actuator and corresponds to a particular wing part. All fragments are influenced by and influence their neighbors through physical links. Chapter 2 brings a trivial example with a one-dimensional system where masses are mentioned as system fragments, and dampings and springs are links between those subsystems. The same idea is applied in Chapters 3 and 4 with different subsystems and links.

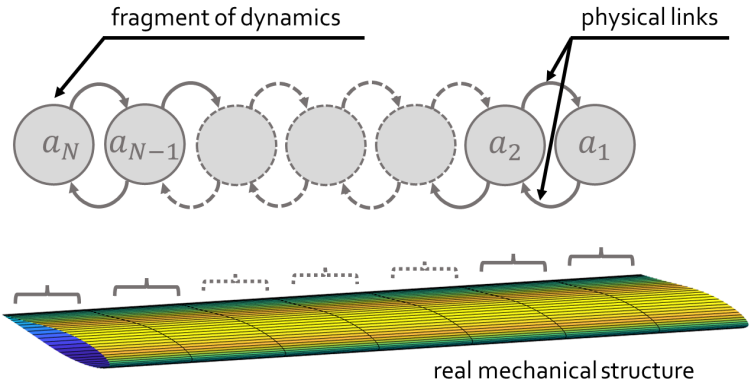

Figure 1.4: Dynamical model interpretation as a group of subsystems with physical links.

The mentioned structured H_∞ control design is also applicable for this type of system. However, for large-scale systems such as flexible morphing wings, an augmented plant with morphing wing model and weighting filters represents a high-order system, making this approach difficult to use. The controller tuning is computationally demanding, and the desired result may not be easily achievable. Therefore, our goal became to find a new approach that could lead to scalable control design easily.

In this thesis, we use benefits arising from the repetitive structure of the system and define control design strategies using just a small system fragment with a model of link and a model of link structure. This approach to a system description is practically identical with the description known from cooperative control theory. The difference is only in the nature of links between the subsystems (*agents*). Compared to our case, where the links between fragments are physical and given, in distributed control theory links between agents are part of the control law and thus/therefore subject to design.

By combining decentralized control with the described flexible systems, we obtain a closed-loop dynamical system with inherent (physics-related) links and control law-related links. This combination can be presented similarly as in Figure 2.1 in Chapter 2. Decentralized control law represents additional connections inside the original system or may even represent connections to the outside of this system. Thereby, we are changing the physical parameters of the flexible system, such as stiffness and damping, or adding extra stiffness and damping between the system and selected airframe components e.g. the fuselage.

Contribution

This thesis is motivated by flexible and morphing wings. We study these system's structures with their properties, and we design new control strategies. Therefore, the key contribution is represented by new algorithms for decentralized control of such systems. Despite our primary motivation, developed algorithms are not limited just to the field of flexible or morphing wings.

The decomposition of large-scale systems into smaller subsystems with common properties allows us to design a control law just for a small fragment of the original system and then propagate the local control law over the whole structure. This approach is known from *Cooperative Control Theory* where a set of *agents* fulfill a common goal. However, agents are usually individual autonomous systems without any physical interconnections. Flexible systems such as morphing wings can similarly be split into smaller parts; nevertheless, neighboring parts affect each other. Thus, results from cooperative control cannot be used directly. Control design algorithms presented in the thesis solve this problem. The resulting approach brings structured control laws with clear physical interpretation. Therefore, the control system scaling or final tuning is simple with the expected behavior.

The goals of this work were achieved and described in the following way. We develop three algorithms for decentralized control low synthesis in Chapters 2,3 and 4. In Chapter 2, an easily scalable control design for decentralized active damping of one-dimensional structure is presented, and thus goal *a)* was achieved. The goal *b)* is related to Chapters 3 and 4, decentralized control synthesis to multi-dimensional flexible structures are developed. In Chapter 3, the decentralized control design has limits depending on physical links inside the system. To solve goal *c)*, where the morphing wing is considered, a third algorithm in Chapter 4 was introduced.

Organization of the thesis

The thesis is organized into three main parts corresponding to journal papers that are already published. Chapter 2 demonstrates the decentralized active damping of one-dimensional structures. We describe this simple model using *Laplacian* and *Kronecker product*. The principle of this description and the role of distributed control law is best seen in this chapter. Decentralized control of more complex structures is presented in Chapter 3 is focused on multi-dimensional large-scale systems. However, the result still has some limitations related to system's degrees of freedom. This is solved in Chapter 4, which introduces a decentralized active damping control for an aeroelastic morphing wing. Finally, the list of author's publications is presented.

2. Low-complexity decentralized active damping of one-dimensional structures

In the paper we propose distributed feedback control laws for active damping of one-dimensional mechanical structures equipped with dense arrays of force actuators and position and velocity sensors. We consider proportional position and velocity feedback from the neighboring nodes with symmetric gains. Achievable control performance with respect to stability margin and damping ratio is discussed. Compared to full-featured complex controllers obtained by modern design methods like LQG, H-infinity or mu-synthesis, these simplistic controllers are more suitable for experimental finetuning, are less case-dependent and they shall be easier to implement on the target future smart-material platforms.

This chapter was published in:
P. Hušek, F. Svoboda, M. Hromčík, Z. Šika, Low-Complexity Decentralized Active Damping of One-Dimensional Structures, Shock and Vibration 2018 (2018) 1-9. doi:10.1155/2018/6421604.

2.1 Introduction

The established paradigm in past and current active damping projects is as follows. The mechanical object is defined first (plate, beam, car-door, wing panel, etc.). Systems detailed design and modelling phases follow [1, 2] giving rise to very accurate FEM models with tens of thousands of degrees of freedom. Alternatively for existing prototypes, the experimental identification approach can be applied to get the mathematical models directly via experimental modal analysis [3]. Model order reduction [1, 4] then gives accurate enough yet tractable models for optimal actuators and sensors placement [5, 6, 7]. Finally a very limited number of them is considered (say up to twenty) for the design of the control laws [1, 8]. Finally, validation and verification of the solutions by high-fidelity simulations is performed, followed by laboratory experiments and final deployment of the product. For any new project - or even a relatively mild modification of a previously accomplished project - all these steps must be performed (or re-visited) again. Implications towards requested research and development costs are significant and obvious.

Therefore there is a need to use another type of control methodologies, and recent advances in MEMS sensors and micro-actuators, ongoing intensive research on new smart materials, and progress in computational power pave the way to massive development of heavily distributed control in this context.

Distributed control is now a very active field of research, thanks to potential applications which require high scalability and reliability. The main advantage of using distributed control is the locality of the necessary measurement and actuation—the measurements are collected and processed in a distributed manner. This kind of control can be applied for automated highway systems [9], car formations [10] and also flexible structures. The work [11]

for instance studies a flexible beam model with bending and torsion motions, and a distributed arrangement with two force-actuators and three moment-actuators paired with rate gyros was elaborated. In [12] a dense network of piezoelectric patch actuators was proposed to realize the distributed actuation. In [13], a distributed piezoelectric actuation was involved and applied to the placement problem of patches so that the deformations are suppressed at pre-selected locations. Multipositive feedback approach for flexible structure control was presented in [14]. Since the flexible systems are passive by nature, one can also employ a lot of results available for distributed control of passive system [15, 16]. Completely passive solutions can be obtained using piezostructures, as reported in [17].

One of the natural goals when dealing with control of flexible mechanical structures is vibration suppression. One standard approach relies on application of a large number of neutralizers placed in prespecified locations along the structure composed from masses and springs. The goal is not only to design the neutralizers' parameters but specify their locations as well since vibrations can be eliminated only at the attachment point of the vibrating beam while amplification of vibration may occur in other parts of the beam. Dynamic vibration absorbers using magnetorheological elastomers were used in [18]. In [19, 20] a set of optimum conditions for global control of the kinetic energy based on the fixed-points theory was proposed. Dynamic transfer matrices using mobility or impedance were used in [21]. In [22] an iterative procedure was developed to find the required resonance frequencies of variable stiffness neutralizers to create nodes at selected locations. Wide-band frequency passive vibration attenuation design for the absorbers was introduced in [23]. In [24] explicit model predictive vibration control was tested. A different approach consists in control and attenuation of multiple travelling waves propagated in a one-dimensional structure [25, 26, 27, 28]. Sliding mode control on seat vibration reduction problem was applied in [29].

2.2 Structured control laws for smart materials

The paper presents an attempt to systematic proportional decentralized position-velocity feedback for active damping of mechanical structures equipped with dense arrays of force actuators and position and velocity sensors. Such a control law is characterized by a very small number of parameters and simple procedures for their tuning compared to centralized approach. Although the results are presented for a one-dimensional structure model only it is believed that a generalization to two-dimensional mechanical structures will be possible.

The research is motivated by vehicular platoon control where relative position and relative or absolute velocity feedback related to the preceding and succeeding vehicle is often considered [30, 31, 32]. Nevertheless, the measure of control performance in both applications is different. For vehicular platooning the main goal consists in preserving a prescribed spacing between the vehicles and in keeping the leader's velocity whereas when dealing with mechanical structures a fast and adequate damping of the oscillating modes is required. Hence the presented control design is focused on investigation of feasible damping ratio of the least damped mode and achievable stability margin of all modes.

Throughout the paper the superscript $\cdot^{\mathrm{T}}$ denotes transpose, I_n stands for $n \times n$ identity matrix, $\mathrm{Re}(\cdot)$ and $\mathrm{Im}(\cdot)$ denotes real and imaginary part, respectively, $\otimes$ denotes the Kronecker product and $\sigma(\cdot)$ denotes the spectrum of a matrix.

2.3 One-dimensional structure longitudinal model

Let us consider a one-dimensional structure composed from the masses m, springs $\bar{k}$ and dampings $\bar{b}$, each of the same value. Let us assume that the

input forces may act on each individual mass independently and we are able to measure positions and velocities of each mass, i.e. actuators and sensors are placed in the same positions. Longitudinal vibrations of such a structure can be described by a state-space model

$$\dot{\bar{x}} = \bar{A}\bar{x} + \bar{B}\bar{u} \tag{2.1}$$

where

$$\bar{x} = [p_1, \dot{p}_1, p_2, \dot{p}_2, \ldots, p_\eta, \dot{p}_\eta]^{\mathrm{T}} \in \Re^{2\eta}, \tag{2.2}$$

$p_i, i = 1, \ldots, \eta$ are the positions of the masses, η is the number of nodes and $\bar{u} \in \Re^{\eta}$ is the vector of the input forces [32].

The matrices $\bar{A} \in \Re^{2\eta \times 2\eta}$ and $\bar{B} \in \Re^{2\eta \times \eta}$ are given by

$$\begin{aligned} \bar{A} &= I_\eta \otimes A_1 + L \otimes A_2, \\ \bar{B} &= I_\eta \otimes ([0\ 1]^{\mathrm{T}}) \end{aligned} \tag{2.3}$$

with

$$A_1 = \begin{bmatrix} 0 & 1 \\ 0 & 0 \end{bmatrix}, A_2 = \begin{bmatrix} 0 & 0 \\ -k_0 & -b_0 \end{bmatrix} \tag{2.4}$$

where $k_0 = \frac{\bar{k}}{m}$, $b_0 = \frac{\bar{b}}{m}$. The matrix $L \in \Re^{\eta \times \eta}$ is the *Laplacian* of the graph

corresponding to the structure which is in this case given as

$$L = \begin{bmatrix} 1 & -1 & & & \\ -1 & 2 & -1 & & \\ & \ddots & \ddots & \ddots & \\ & & -1 & 2 & -1 \\ & & & -1 & 1 \end{bmatrix}. \tag{2.5}$$

Since for practical reasons at least one of the nodes has to be fixed the equation (2.1) becomes

$$\dot{x} = Ax + Bu \tag{2.6}$$

where $x \in \Re^{2n}$, $u \in \Re^n$ come from $\bar{x}$ and $\bar{u}$ by omitting the entries corresponding to the fixed nodes and n is the number of the non-fixed nodes.

The matrices $A \in \Re^{2n \times 2n}$ and $B \in \Re^{2n \times n}$ are then given by

$$\begin{aligned} A &= I_n \otimes A_1 + L_{\mathrm{g}} \otimes A_2, \\ B &= I_n \otimes ([0\ 1]^{\mathrm{T}}) \end{aligned} \tag{2.7}$$

where the matrix $L_{\mathrm{g}} \in \Re^{n \times n}$ is called the *grounded* Laplacian that results from Laplacian L (2.5) by omitting the rows and columns corresponding to the fixed nodes. In the sequel we will assume without loss of generality that the fixed nodes are the first and last one, $n = \eta - 2$ and

$$L_{\mathrm{g}} = \begin{bmatrix} 2 & -1 & & & \\ -1 & 2 & -1 & & \\ & \ddots & \ddots & \ddots & \\ & & -1 & 2 & -1 \\ & & & -1 & 2 \end{bmatrix}. \tag{2.8}$$

The eigenvalues of L_g are all positive and are given by

$$\lambda_\ell = 2 - 2\cos\left(\frac{\ell\pi}{n+1}\right), \ell = 1,\ldots,n. \tag{2.9}$$

We will see later that from the eigenvalues (2.9) the minimum and maximum ones are of special interest. Those can be determined as

$$\lambda_{\min} = \min_\ell \lambda_\ell = \lambda_1 = 2 - 2\cos\left(\frac{\pi}{n+1}\right), \tag{2.10}$$

$$\lambda_{\max} = \max_\ell \lambda_\ell = \lambda_n = 2 - 2\cos\left(\frac{n\pi}{n+1}\right). \tag{2.11}$$

In this paper we will use distributed control law where the control action applied to each node depends symmetrically on relative positions and velocities with respect to its neighbors, i.e.

$$\begin{aligned} u_i &= -k(p_{i+1} - p_i) - k(p_{i+1} - p_{i+2}) - b(\dot{p}_{i+1} - \dot{p}_i) - b(\dot{p}_{i+1} - \dot{p}_{i+2}), \\ i &= 1,\ldots,n, \quad k,b \geq 0 \end{aligned} \tag{2.12}$$

with p_1 and p_{n+2} being fixed, see Fig. 2.1.

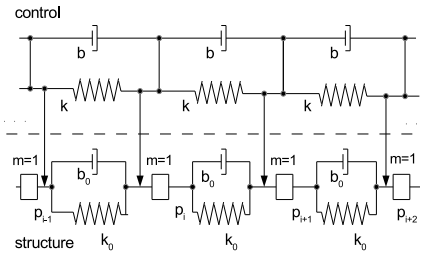

Figure 2.1: Distributed control law of a one-dimensional structure

The control law (2.12) can be written as

$$u = Kx = (L_{\mathrm{g}} \otimes [k \ b])x. \tag{2.13}$$

After substituting (2.13) into (2.6) one obtains the description of the closed-loop system

$$\dot{x} = A_{\mathrm{c}}x = (A + BK)x \tag{2.14}$$

where

$$A + BK = I_n \otimes A_1 + L_{\mathrm{g}} \otimes A_2 + L_{\mathrm{g}} \otimes K_2 = I_n \otimes A_1 + L_{\mathrm{g}} \otimes (A_2 + K_2) \tag{2.15}$$

with

$$K_2 = \begin{bmatrix} 0 & 0 \\ -k & -b \end{bmatrix}. \tag{2.16}$$

For determination of the eigenvalues of matrix A_{c} we will use the following lemma.

Lemma [32].

$$\sigma(I_n \otimes \tilde{A}_1 + \tilde{L} \otimes \tilde{A}_2) = \bigcup_{\lambda_\ell \in \sigma(\tilde{L})} \{\sigma(\tilde{A}_1 + \lambda_l \tilde{A}_2)\}. \tag{2.17}$$

□

Using lemma 1 we immediately obtain the following result:

$$\sigma(A_{\mathrm{c}}) = \sigma(I_n \otimes A_1 + L_{\mathrm{g}} \otimes (A_2 + K_2)) = \bigcup_{\lambda_\ell \in \sigma(L_{\mathrm{g}})} \left\{ \sigma \begin{bmatrix} 0 & 1 \\ -\lambda_\ell(k_0 + k) & -\lambda_\ell(b_0 + b) \end{bmatrix} \right\}. \tag{2.18}$$

It turns out that the closed-loop eigenvalues are given as the roots of the characteristic equation

$$s^2 + \lambda_\ell(b_0 + b)s + \lambda_\ell(k_0 + k) = 0, \ell = 1, \ldots, n \tag{2.19}$$

i. e.

$$s_\ell^{\pm} = \frac{-\lambda_\ell(b_0 + b) \pm \sqrt{\lambda_\ell^2(b_0 + b)^2 - 4\lambda_\ell(k_0 + k)}}{2}, \ell = 1, \ldots, n. \tag{2.20}$$

2.4 Control strategies

There are many options where to place the closed-loop eigenvalues. Nevertheless, from the vibration suppression point of view the following two are the most interesting ones.

2.4.1 Prescribed damping ratio

A quite natural option is to force all modes to be damped with a prescribed minimum damping ratio $\zeta_{\min} \in [0, 1]$. From (2.20) one can see that if k is fixed then with increasing value of b the least damped mode is that corresponding to $\lambda_{\min}$. The ratio of imaginary and real part of the least damped mode that corresponds to $\lambda_{\min}$ is given by

$$\xi_{\max} = \left| \frac{\mathrm{Im}(s_1)}{\mathrm{Re}(s_1)} \right| = \frac{\sqrt{4\lambda_{\min}(k_0 + k) - \lambda_{\min}^2(b_0 + b)^2}}{\lambda_{\min}(b_0 + b)}. \tag{2.21}$$

Hence the minimum value of b satisfying this condition is given by

$$b_{\mathrm{damp}} = \sqrt{\frac{4(k_0 + k_{\mathrm{damp}})}{\lambda_{\min}(\xi_{\max}^2 + 1)}} - b_0 \tag{2.22}$$

where k_{damp} is set arbitrarily.

Since the corresponding damping ratio is given as

$$\zeta_{\min} = \sqrt{\frac{1}{1+\xi_{\max}^2}} \tag{2.23}$$

after substitution into (2.22) we obtain

$$b_{\text{damp}} = 2\zeta_{\min}\sqrt{\frac{k_0+k_{\text{damp}}}{\lambda_{\min}}} - b_0. \tag{2.24}$$

Let us define stability margin as

$$\delta = \min_{\ell} |\text{Re}(s_\ell)|. \tag{2.25}$$

Stability margin of such a control law is determined by the distance of the least and most damped closed-loop eigenvalues, s_1 and s_n^+, respectively, from the imaginary axis for $b = b_{\text{damp}}, k = k_{\text{damp}}$. The distance of complex conjugate $s_1^\pm$ corresponding to $\lambda_{\min}$ whose position is given by the prescribed damping ratio is given by

$$d(s_1^\pm) = -\text{Re}(s_1) = \frac{\lambda_{\min}(b_0+b_{\text{damp}})}{2} \tag{2.26}$$

whereas distance of real s_n^+ corresponding to $\lambda_{\max}$ can be obtained as

$$d(s_n^+) = \frac{\lambda_{\max}(b_0+b_{\text{damp}}) - \sqrt{\lambda_{\max}^2(b_0+b_{\text{damp}})^2 - 4\lambda_{\max}(k_0+k_{\text{damp}})}}{2} \tag{2.27}$$

Stability margin is then given as minimum of (2.26) and (2.27),

$$d_{\text{damp}} = \min\{d(s_1^\pm), d(s_n^+)\} \tag{2.28}$$

which after some algebraic manipulations yields

$$d_{\text{damp}} = \min\left\{ \zeta_{\min}\lambda_{\min}\sqrt{k_0 + k_{\text{damp}}}, \right.$$
$$\left. \sqrt{\lambda_{\max}(k_0 + k_{\text{damp}})}\left(\zeta_{\min}\sqrt{\frac{\lambda_{\max}}{\lambda_{\min}}} - \sqrt{\zeta_{\min}^2 \frac{\lambda_{\max}}{\lambda_{\min}} - 1} \right) \right\}. \tag{2.29}$$

It should be noted that for very small damping ($\zeta_{\min} < \frac{\lambda_{\min}}{\lambda_{\max}}$) the eigenvalue s_n is not real and the second term in (2.29) becomes complex and should not be considered. Nevertheless, considering such a small damping is highly impractical.

The dependence of stability margin on prescribed minimum damping ratio given by (2.29) for $n = 48$ and $k_0 + k_{\text{damp}} = 1$ is depicted in Fig. 2.2.

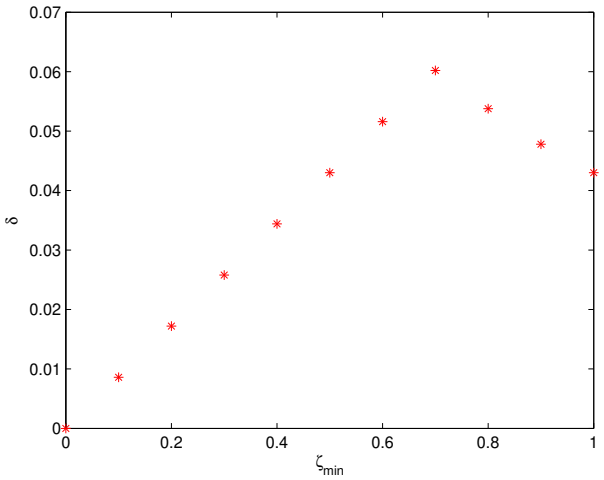

Figure 2.2: Stability margin dependence on damping ratio

2.4.2 Maximum stability margin

Another interesting option is to find the control parameters that maximize the stability margin (2.25). From (2.20) it follows that the stability margin of the eigenvalues lying on real axis is determined by that corresponding to $\lambda_{\max}$ and stability margin of the eigenvalues lying out of real axis is determined by those corresponding to $\lambda_{\min}$. Thus the maximum stability margin is achieved if

$$\mathrm{Re}(s_1^{\pm}) = \mathrm{Re}(s_n^{+}) \tag{2.30}$$

where s_1 and s_n are the eigenvalues corresponding to $\lambda_{\min}$ and $\lambda_{\max}$, respectively.

Condition (2.30) can be written as

$$-\lambda_{\min}(b_0+b) = -\lambda_{\max}(b_0+b) + \sqrt{\lambda_{\max}^2(b_0+b)^2 - 4\lambda_{\max}(k_0+k)} \tag{2.31}$$

from which we obtain

$$b_{\mathrm{marg}} = \sqrt{\frac{4\lambda_{\max}(k_0+k_{\mathrm{marg}})}{\lambda_{\min}(2\lambda_{\max}-\lambda_{\min})}} - b_0 \tag{2.32}$$

for arbitrarily chosen k_{marg}.

By substituting (2.32) in (2.30) we obtain the maximum stability margin as

$$\delta_{\max} = \sqrt{k_0+k_{\mathrm{marg}}}\sqrt{\frac{\lambda_{\max}\lambda_{\min}}{2\lambda_{\max}-\lambda_{\min}}}\,. \tag{2.33}$$

The ratio of imaginary and real part of the least damped mode that corre-

sponds to $\lambda_{\min}$ is given by

$$\xi_{\max} = \left| \frac{\mathrm{Im}(s_1)}{\mathrm{Re}(s_1)} \right| = \frac{\sqrt{4\lambda_{\min}(k_0 + k_{\mathrm{marg}}) - \lambda_{\min}^2 (b_0 + b_{\mathrm{marg}})^2}}{\lambda_{\min}(b_0 + b_{\mathrm{marg}})} \tag{2.34}$$

that yields after substitution from (2.32) and some simplifications

$$\xi_{\max} = \sqrt{1 - \frac{\lambda_{\min}}{\lambda_{\max}}}\,. \tag{2.35}$$

From that the damping ratio of the least damping mode follows as

$$\zeta_{\min} = \sqrt{\frac{1}{1 + \xi_{\max}^2}} = \sqrt{\frac{\lambda_{\max}}{2\lambda_{\max} - \lambda_{\min}}}\,. \tag{2.36}$$

The achievable stability margins for different values of n for both approaches are shown in Fig. 2.3 whereas the minimum damping ratio corresponding to maximum stability margin is depicted in Fig. 2.4. Both figures are plotted for $k_0 + k_{\mathrm{marg}} = 1$.

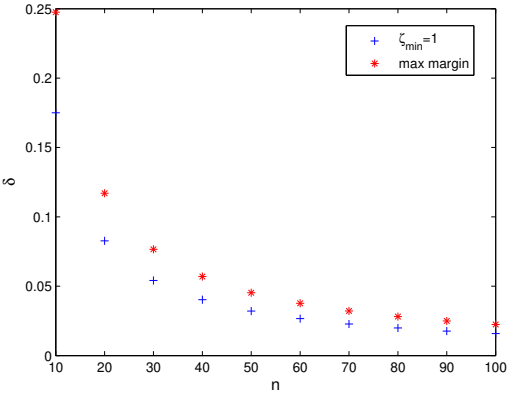

Figure 2.3: Comparison of stability margins of both approaches depending on number of nodes

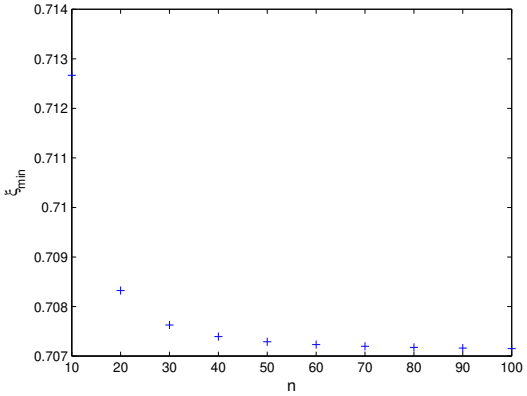

Figure 2.4: Minimum damping ratio for maximum stability margin approach depending on number of nodes

2.5 Example

Let us illustrate the results derived in the previous section on an example. We will consider the following parameters: $m = 5 \cdot 10^{-4}\,\mathrm{kg}, \bar{b} = 3.3 \cdot 10^{-3}\,\mathrm{Ns/m}$; $\bar{k} = 0.4\,\mathrm{N/m}$, $n = 48$. We set the control parameter $k = k_{\mathrm{damp}} = k_{\mathrm{marg}} = 10\,\mathrm{N/m}$.

The minimum and maximum eigenvalues of the grounded Laplacian become

$$\begin{aligned} \lambda_{\min} &= 2 - 2\cos\left(\frac{\pi}{n+1}\right) = 0.0041, \\ \lambda_{\max} &= 2 - 2\cos\left(\frac{n\pi}{n+1}\right) = 3.99\,. \end{aligned}$$

The minimum value of $b = b_{\mathrm{damp}}$ damping all the eigenvalues with minimum damping ratio $\zeta_{\min} = 0.6$ is given by

$$b_{\mathrm{damp}} = 2\zeta_{\min}\sqrt{\frac{k_0 + k_{\mathrm{damp}}}{\lambda_{\min}}} - b_0 = 527\,\mathrm{s}^{-1}\,.$$

Such a control law guarantees the stability margin

$$\delta_{\mathrm{damp}} = \min\{1.521, 1.095\} = 1.095\,.$$

The position of dominant open- and closed-loop eigenvalues is plotted in Fig. 2.5.

The value of control parameter b guaranteeing maximum stability margin yields

$$b_{\mathrm{marg}} = \sqrt{\frac{4\lambda_{\max}(k_0 + k_{\mathrm{marg}})}{\lambda_{\min}(2\lambda_{\max} - \lambda_{\min})}} - b_0 = 622\,\mathrm{s}^{-1}$$

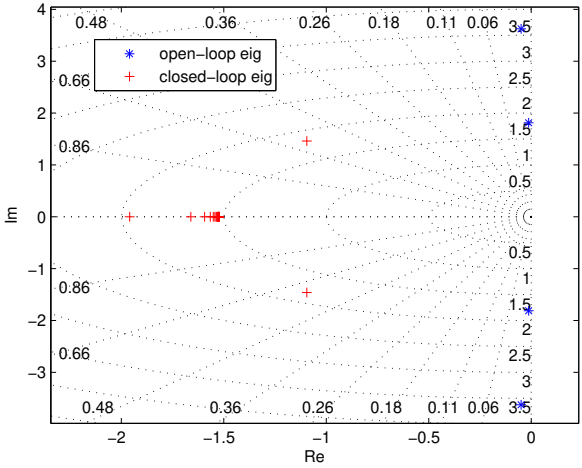

Figure 2.5: Dominant modes for minimum damping ratio $\zeta_{\min} = 0.6$

corresponding to stability margin

$$\delta_{\max} = \sqrt{k_0 + k_{\text{marg}}} \sqrt{\frac{\lambda_{\max}\lambda_{\min}}{2\lambda_{\max} - \lambda_{\min}}} = 1.29.$$

Damping ratio of the least damped mode is given by

$$\zeta_{\min} = \sqrt{\frac{\lambda_{\max}}{2\lambda_{\max} - \lambda_{\min}}} = 0.707\,.$$

The corresponding position of dominant open- and closed-loop eigenvalues is depicted in Fig. 2.6.

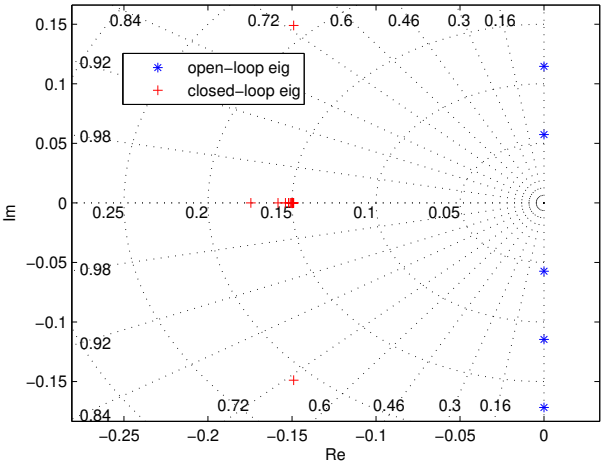

Figure 2.6: Dominant modes for maximum stability margin appraoch

To demonstrate the presented design we compare time and frequency responses of a point lying in the middle of the beam for different values of damping ratios. The open-loop responses to initial condition $p_i(0) = 0.01\,\mathrm{m}$, $\dot{p}_i(0) = 0, i = 1,\ldots,n$ are shown in Fig. 2.7.

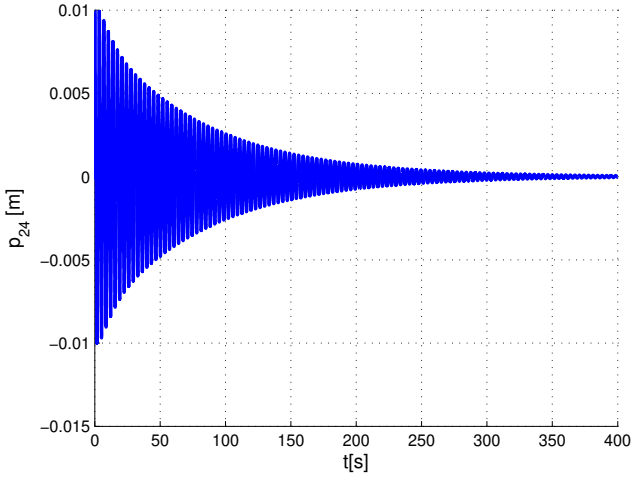

Figure 2.7: Initial condition displacement response of uncontrolled structure

The initial condition response for different prescribed minimum damping ratios are depicted in Fig. 2.8. The Bode plots are compared in Fig. 2.9.

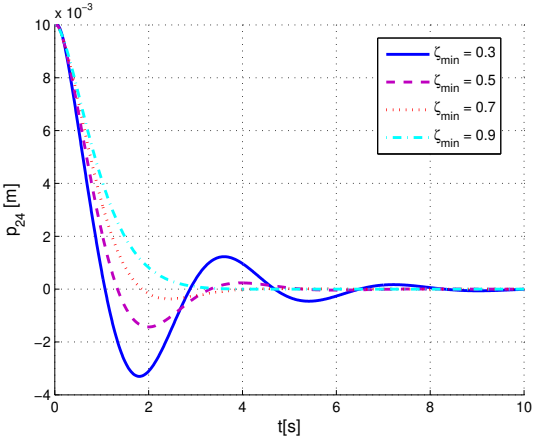

Figure 2.8: Initial condition displacement response for different damping ratios

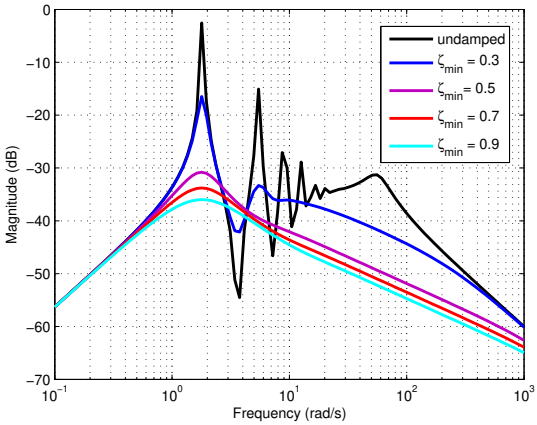

Figure 2.9: Bode plot for different prescribed minimum damping ratios

Let us compare the achieved results with other two standard design methods typically used by the control community. At first we design an LQ controller with relative positions and velocities considered as measurable state variables, i. e.

$$\begin{aligned} u_i &= \sum_{j=1}^{n} \Big(-k_{ij}(p_{j+1}-p_j) - k_{ij}(p_{j+1}-p_{j+2}) - b_{ij}(\dot{p}_{j+1}-\dot{p}_j) \\ &- b_{ij}(\dot{p}_{j+1}-\dot{p}_{j+2}) \Big), i = 1,\ldots,n. \end{aligned}$$

The difference between the LQ and presented control law is that the LQ control law uses relative positions and velocities between all neighbouring nodes and not between the closest neighbors only as in (2.12). To force the LQ control to use relative positions and velocities we introduce a modified state vector

$$\begin{aligned} z = [&p_2 - p_1 + p_2 - p_3, \dot{p}_2 - \dot{p}_1 + \dot{p}_2 - \dot{p}_3, \ldots, p_{n+1} - p_n + p_{n+1} - p_{n+2}, \\ &\dot{p}_{n+1} - \dot{p}_n + \dot{p}_{n+1} - \dot{p}_{n+2}]^{\mathrm{T}}. \end{aligned}$$

The criterion to be minimized is then given by

$$J = \int_0^\infty (z^{\mathrm{T}} Q z + u^{\mathrm{T}} R u) dt$$

resulting in LQ feedback control law

$$u = Kz$$

with

$$K = \begin{bmatrix} k_{22} & b_{22} & k_{23} & b_{23} & \cdots & k_{2n+1} & b_{2n+1} \\ k_{32} & b_{32} & k_{33} & b_{33} & \cdots & k_{3n+1} & b_{3n+1} \\ \vdots & \vdots & \vdots & \vdots & \cdots & \vdots & \vdots \\ k_{n+12} & b_{n+12} & k_{n+13} & b_{n+13} & \cdots & k_{n+1n+1} & b_{n+1n+1} \end{bmatrix}.$$

By tuning the weighting matrices Q and R to guarantee minimum damping ratio $\zeta_{\min} = 0.6$ we obtained the corresponding stability margin $\delta_{\text{damp}} = 1.162$, see dominant poles in Fig. 2.10. Tuning the weighting matrices to maximize stability margin we arrived to $\delta_{\max} = 1.01$ with corresponding $\zeta_{\min} = 0.903$ that can be seen from dominant poles in Fig. 2.11. Hence the dominant poles configuration is very similar to the proposed design (Fig. 2.5 and Fig. 2.6).

The control gains k_{ij} and b_{ij} for the former case are depicted in Fig. 2.12 and Fig. 2.13, respectively. One can see that the control law uses the relative positions and velocities to the closest neighbors only and that the gains are almost the same for all nodes.

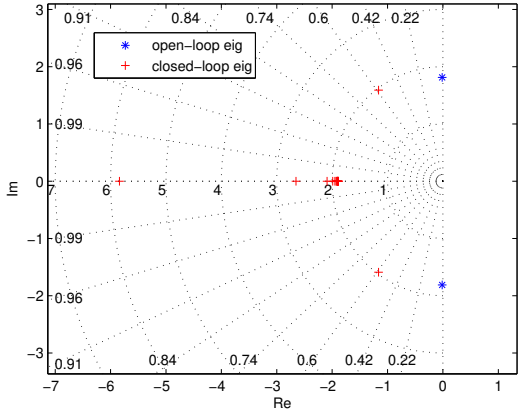

Figure 2.10: Dominant poles for LQ controller design, $\zeta_{\min} = 0.6$

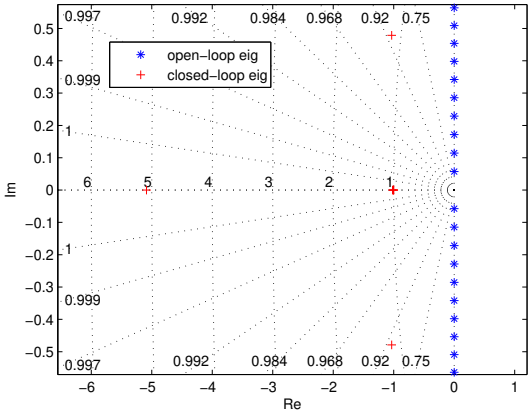

Figure 2.11: Dominant poles for LQ controller design – maximum stability margin

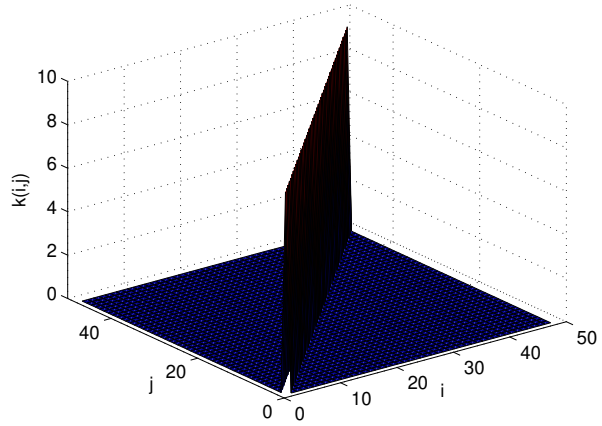

Figure 2.12: Control gains k_{ij} for LQ controller design, $\zeta = 0.6$

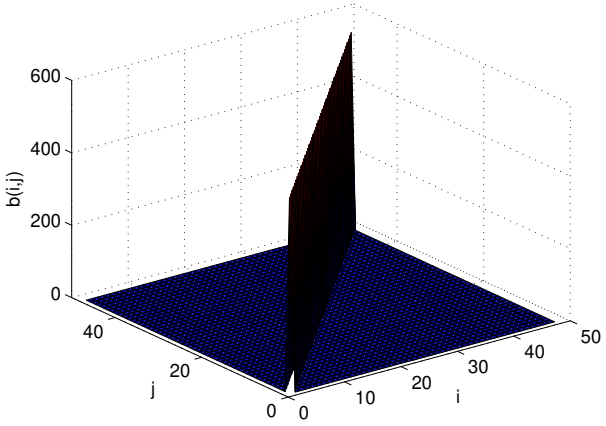

Figure 2.13: Control gains b_{ij} for LQ controller design, $\zeta = 0.6$

To compare our methodology with another control design approach, we formulated the task as an H_∞ design for the fixed structure controller (2.12). It can be easily done with *hinfstruct()* function in Matlab Robust Control Toolbox. This tuning minimizes the H_∞ norm of the closed-loop transfer function modeled by the closed-loop control system with tunable components and weighting filters. In our case, the high-pass filter with cutoff frequency 8 rad/s has been used to penalize all system modes.

The H-infinity design methodology offers efficient algorithms how to obtain multivariable control laws by specifying closed-loop frequency response requirements. This approach was used e.g. in [33], where authors compare classical single-input single-output controllers with H-infinity approaches in terms of robustness and performance. The order of the H-infinity control system is however equal to the so called augmented plant containing the model of the controlled system along with the weighting filters defining performance and robustness requirements. This leads to excessively high order control laws typically, with strong negative impact on implementation and experimental fine-tuning. For this reason, in e.g. [34] there was a method presented for the controller order reduction which is one possible way how to get control laws with reasonable complexity. Nevertheless, loss or deterioration of closed-loop performance and/or stability is often an unwanted effect associated with this approach. Thanks to recent structured H-infinity control synthesis results, see e.g. [35, 36] it is possible to receive the parameters of such reduced-order controllers directly, minimizing the H-infinity norm under the controller complexity constraints.

The Bode plots of original system, LQ controller tuned for prescribed minimum damping ratio $\zeta_{\min} = 0.6$, the H_∞ controller and the proposed design for $\zeta_{\min} = 0.6$ are compared in Fig. 2.14. The plots confirm that all designs give very similar results.

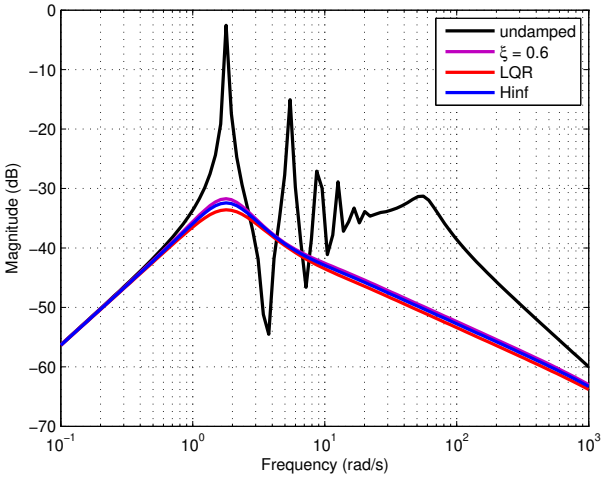

Figure 2.14: Bode plot for displacement for different control strategies

2.6 Conclusion

In the paper we presented an active approach of one-dimensional structures with dense array of collocated sensors and actuators using proportional position and velocity feedback control laws. The control law was formulated in a distributive manner, i.e. each actuator uses information from its closest neighbors only. The achievable stability margins and damping ratios were analyzed based on the properties of Laplacian matrix describing the corresponding information graph. Comparison with LQ controller and H_∞ designs shows that the presented approach achieves similar results yet with much lower computational and actuator complexity.

References

[1] M. Kozek and A. Schirrer (Eds.), Modeling and Control for a Blended Wing Body Aircraft, Springer, 2015.

[2] R. R. Craig, Coupling of Substructures for Dynamic Analyses: An Overview, in: 41st Structures, Structural Dynamics, and Materials Conference and Exhibit, Atlanta, Georgia, 2000, pp. AIAA–2000–1573.

[3] P. Verboven, Frequency-domain system identification for modal analysis, Ph.D. thesis, Mechanical Engineering Department (WERK), Brussels: Vrije Universiteit Brussel (2002).

[4] W. K. Gawronski, Advanced Structural Dynamics and Active Control of Structures, Springer-Verlag New York, Inc., 2004.

[5] T. Haniš, M. Hromčík, Optimal sensors placement and spillover suppression, Mech. Syst. Signal Process. 28 (19) (2012) 367–378.

[6] D. C. Kammer, M. L. Tinker, Optimal placement of triaxial accelerometers for modal vibration tests, Mech. Syst. Signal Process. 18 (2004) 29–41.

[7] W. Liu, Z. Hou, M. A. Demetriou, A computational scheme for the optimal sensor/actuator placement of flexible structures using spatial H2 measures, Mech. Syst. Signal Process. 20 (2006) 881–895.

[8] M. Alam, M. Hromčík, T. Haniš, Active gust load alleviation system for flexible aircraft: Mixed feedforward/feedback approach, Aerosp. Sci. Technol. 41 (2015) 122–133.

[9] J. K. Hedrick, M. Tomizuka, P. Varaiya, Control issues in automated highway systems, IEEE Contr. Syst. Mag. 14 (1994) 21–32.

[10] S. Darbha, P. R. Pagilla, Limitations of employing undirected information flow graphs for the maintenance of rigid formations for heterogeneous vehicles, Int. J. Eng. Sci. 48 (11) (2010) 1164–1178.

[11] W. W. Zhang, Root locus approach to a distributed parameter vibrating system with both bending and torsion motions, Int. J. Mech. Sci 37 (6) (1995) 585–600.

[12] M. Krommer, H. Irschik, M. Zellhofer, Design of Actuator Networks for Dynamic Displacement Tracking of Beams, Mech. Adv. Mater. Struc. 15 (2008) 235–249.

[13] H. Irschik, M. Nader, Actuator placement in static bending of smart beams utilizing Mohrs Analogy, Mech. Adv. Mater. Struc. 31 (8) (2009) 1698–1706.

[14] E. Omidi, S. N. Mahmoodi, W. S. Shepard, Multi positive feedback control method for active vibration suppression in flexible structures, Mechatronics 33 (2016) 23–33.

[15] L. Gaul, J. Becker, Reduction of Structural Vibrations by Passive and Semiactively Controlled Friction Dampers, Shock Vib. 4 (2014) 1–7.

[16] D. Hughes, J. T. Wen, Passivity motivated controller design for flexible structures, J. Guid. Control Dynam. 19 (3) (1996) 726–729.

[17] D. Halim, S. O. R. Moheimani, Spatial resonant control of flexible structures-application to a piezoelectric laminate beam, IEEE T. Contr. Syst. T. 9 (1) (2001) 37–53.

[18] T. Komatsuzaki, T. Inoue, O. Terashima, Broadband vibration control of a structure by using a magnetorheological elastomer-based tuned dynamic absorber, Mechatronics 40 (2016) 128–136.

[19] J. Dayou, S. M. Kim, Control of kinetic energy of a one-dimensional structure using multiple vibration neutralizers, J. Sound Vib. 281 (2005) 323–340.

[20] J. Dayou, Fixed-points theory for global vibration control using vibration neutralizer, J. Sound Vib. 262 (2006) 765–776.

[21] R. Chen, T. Wu, Vibration control of base system using distributed dynamic vibration absorbers, J. Vib. Control 2 (10) (2014) 1589–1600.

[22] S. S. Patil, P. J. Awasare, Vibration reduction at desired locations on a beam by creating nodes using tunable vibration neutralizers, J. Vib. Control 22 (1) (2016) 205–223.

[23] M. Azoulay, A. Veprik, V. Babitsky, N. Halliwell, Distributed absorber for noise and vibration control, Shock Vib. 18 (2011) 181–219.

[24] G. Takacs, G. Batista, M. Gulan, B. Rohal-Ilkiv, Embedded explicit model predictive vibration control, Mechatronics 36 (2017) 54–62.

[25] P. Gardonio, S. J. Elliott, Active control of waves on a one-dimensional structure with a scattering termination, J. Sound Vib. 192 (3) (1996) 701–730.

[26] R. Gabai, I. Bucher, Excitation and sensing of multiple vibrating traveling waves in one-dimensional structures, J. Sound Vib. 319 (1-2) (2009) 406–425.

[27] F. Li, C. Zhang, C. Liu, Active tuning of vibration and wave propagation in elastic beams with periodically placed piezoelectricactuator/sensor pairs, J. Sound Vib. 393 (2017) 14–29.

[28] S. Chen, G.Wang, J.Wen, X.Wen, Wave propagation and attenuation in plates with periodic arrays of shunted piezo-patches, J. Sound Vib. 332 (2013) 15201532.

[29] D. Ning, S. Sun, L. Wei, B. Zhang, W. Li, Vibration reduction of seat suspension using observer based terminal sliding mode control with acceleration data fusion, Mechatronics 44 (2017) 71–83.

[30] Y. Zhang, B. Kosmatopoulos, P. Ioannou, C. Chien, Using front and back information for tight vehicle following maneuvers, IEEE T. Veh. Technol. 48 (1) (1999) 319–328.

[31] P. Barooah, P. G. Mehta, J. P. Hespanha, Mistuning-based decentralized control of vehicular platoons for improved closed loop stability, IEEE T. Automat. Contr. 54 (9) (2009) 2100–2113.

[32] H. Hao, P. Barooah, On Achieving Size-Independent Stability Margin of Vehicular Lattice Formations With Distributed Control, IEEE T. Automat. Contr. 57 (10) (2012) 2688–2694.

[33] M. R. Waszak, Robust Multivariable Flutter Suppression for Banchmark Active Control Technology Wind-Tunnel Model, Journal of Guidance, Control, and Dynamics (2001) 147–153.

[34] A. Varga, Balancing Free Square-root Algorithm for Computing Singular Perturbation Approximations, in: in 30th Conference on Decision and Control, Brighton, UK, 1991.

[35] P. Apkarian, D. Noll, Nonsmooth H-infinity Synthesis, IEEE Transactions on Automatic Control (2006) 71–86.

[36] S. Gumussoy, D. Henrion, M. Millstone, M. L. Overton, Multiobjective Robust Control with HIFOO 2.0, in: in Proceedings of the IFAC Symposium on Robust Control Design, Haifa, Israel, 2009.

3. Decentralized control for large scale systems with inherently coupled subsystems

This paper brings a novel scalable control design methodology for Large-Scale Systems (LSS). Such systems are considered as multi-agent systems with inherent interactions between neighboring agents. The presented design methodology uses single-agent dynamics and their interaction topology, rather than relying on the model of the entire system. The dimension of the design problem therefore remains the same with growing number of agents. This allows a feasible control design even for large systems. Moreover, the proposed design is based on simple Linear Matrix Inequalities (LMI), efficiently solvable using standard computational tools. Numerical results validate the proposed approach.

This chapter was published in:
F. Svoboda, K. Hengster-Movric, M. Hromčík, Decentralized control for large scale systems with inherently coupled subsystems, Journal of Vibration and Control 28 (23-24) (2022) 3931-3938.
doi:10.1177/10775463211034953

3.1 Introduction

Large-scale systems (LSS) appear in a wide range of engineering applications, including chemical processes [1], thermo systems [2], flexible structures [3], to name just a few.[4] Such a variety of systems brings diverse analysis methods and control design approaches [5]. A survey of conventional control methods for LSS is presented in [4], [6]. For easier orientation, existing approaches can be classified according to:

- *Control system structure*
  centralized or decentralized control
- *System type*
  unstructured LSS without a given internal structure; multi-agent system with inherently independent single-agent dynamics; or interconnected LSS with a specific structure
- *Model used for controller design*
  a model of the entire system; or a model structure only, with appropriately partitioned system.

Control of complex phenomena, modeled within a common framework of LSS, is often found challenging due to demands on computational resources and efficient model utilization [7]. Model order reduction and centralized control are the usual responses to these issues, where typically a lower-order design model replicates the original high-order model, thus reducing the design effort. There are several model order reduction techniques available in the literature [4, 8]. However, this approach brings new problems associated with a lack of stability guarantees, with a reduced-model no longer interpolating the original one, but rather a model approximating it, or with the model

[4] Refer e.g. to [4] for a more complete survey.

reduction being computationally difficult. Depending on system complexity, other centralized approaches, [9], also suffer from computational issues.

Cooperative control presents another option. It conventionally deals with distributed protocols and agent-based dynamical models. Studied systems consist of autonomous subsystems, called *agents* [10], each of which addresses, in a coordinated manner, a specific sub-task to attain the overall design objective. Due to many potential applications requiring scalability and reliability, cooperative control remains a very active field of research examining collective behavior of autonomous subsystems. A cooperative multi-agent system is commonly described by a graph, with nodes representing dynamical subsystems and edges representing interactions between them, [11]. The extensively researched canonical problems in cooperative control of multi-agent systems are *consensus* and *synchronization*, [12]. However, those are typically studied for systems without any inherent interactions between the subsystems; the controller alone ensuring agent interactions, as usually found in mobile robot formations, multi-vehicle systems, etc. The applied control laws in those cases thus form a distributed virtual connection between the originally uncoupled agents. In particular, [13] proposes a framework for synchronization of cooperative systems via full state-feedback. This allows designing stabilizing cooperative state-feedback controllers based only on single-agent dynamics and the pertaining local algebraic Riccati equation. Synchronization using dynamic compensators or output-feedback is presented in [12, 14]. Furthermore, [15] or [16] consider optimality of cooperative control protocols with respect to a global quadratic performance criterion.

Nevertheless, as multi-agent systems considered in cooperative control originally have independent single-agent dynamics, conventional cooperative control results unfortunately do not extend straightforwardly to systems having inherent interconnections between subsystems such as naturally arise in e.g. electric power systems, flexible structures, heat transfer with multiple

heat sources, and many other distributed systems [17].

Other computationally attractive control designs for distributed LSS rest on linear matrix inequalities (LMIs). In particular, [18] brings an LMI approach to decentralized control for distributed parameter systems having a specific structure. However, this result is generally conservative, and it relies on the entire system model. Similarly, [19], [20] also present a decentralized control design with a model of the entire system. For large systems, (having many agents), using the entire system model for control design often leads to computationally infeasible solutions. In contrast, [21] considers the detailed structure of a multi-agent system with inherently coupled agents for control design, providing decentralized state-feedback to minimize the effects of subsystem interactions and to guarantee the stability of the whole system. Despite using the system structure, the method proposed in [21] is found to be conservative, scaling rather unfavorably with a growing number of agents. In [22] and [23] a flexible structure is decomposed into N coupled subsystems, and decentralized control of one-dimensional structures is subsequently examined. Both latter approaches only consider one-dimensional structures, which ultimately limits their applicability. The special structure of coupled multi-agent systems is also assumed in [24], where a passive dynamical system interconnects the agents. This interconnection contains integrators, so a direct connection between agent states is not considered. Distributed control for dynamically coupled systems is presented in [25] where the controller has the same interconnection structure as the system. However, this methodology can be used only for discrete-time systems of special structure - namely, they need to be *decomposable* (see [25], page 125, definition 4, for the definition of decomposable systems).

This paper considers a broad class of systems, including various plants composed of several coupled subsystems. In aerospace, civil engineering, and many other areas, we can find flexible structures where vibrations are un-

desirable and need to be attenuated. In [22] the authors address the problem of designing stabilizing controllers for cable-stayed flexible structures such as bridges. Cooperative control for distributed morphing wing systems is proposed in [26]. Another application in this class of systems is parameter control in production processes. For example, a paper machine uses an array of actuators that compensate for irregularities in the paper pulp distribution on a conveyor belt [25]. In formation flying problems, plants are typically dynamically disconnected subsystems. However, the cross-coupling between them is introduced by the performance index. The paper [25] presents distributed control of a satellite formation on a circular orbit where the performance index penalizes the satellite position difference.

A computationally favorable control design methodology for systems with inherently directly coupled subsystems, based on single-agent dynamics akin to that found in cooperative control theory, is thus still lacking. Therefore, the objective of this paper, in contrast to existing results, is to develop a decentralized control design for LSS by exploiting recurrence and symmetry typical for flexible structures. Such design is required to scale well with the number of agents, remaining computationally feasible for LSS. For that purpose, the target dynamical systems are understood as multi-agent systems [12] with inherent couplings between neighboring agents, independent of any applied controls. This differs from conventional multi-agent systems, which are coupled only through applied controls [11, 13], while also differing from designs based on entire system models by using agents in a distributed way. The resulting closed-loop stability condition for decentralized static state-feedback is presented as an LMI, [27], which can be solved efficiently using standard numerical procedures. Thus, this paper merges LSS control design with results from cooperative control, making use of standard LMI methods to provide an efficient, scalable, and distributed design for LSS.

The paper is organized as follows: preliminaries are given in Section 3.2.

Section 3.3 considers the system structure and presents the structure of the control law. The main result, an LMI control design, is derived in Section 3.4. Section 3.5 brings two examples of a flexible structure. The proposed design is compared with existing design methods, and simple controller tuning precepts are given. Section 3.6 concludes the paper.

3.2 Preliminaries

In this paper, various distributed and decentralized control approaches are discussed. Let us emphasize from the outset that these terms, although used synonymously in some texts, actually describe two distinct approaches. A decentralized controller consists of local independent controllers for individual parts of the plant (agents). If local controllers also share information with their neighbors, then we talk about distributed control.

Notation: $I_N \in \mathbb{R}^{N\times N}$ is the identity matrix. Kronecker product is denoted by $\otimes$. $L = [l_{ij}]$ is a matrix with entry l_{ij} on ith row and jth column. $D = \text{diag}\{d_i\}$ is a diagonal matrix with entries d_i. By $Q > 0$ ($Q < 0$) we denote that the matrix Q is positive (negative) definite. $\lambda_i(M)$ are eigenvalues of matrix M. The maximum (minimum) eigenvalues are denoted by $\overline{\lambda}(M)$ ($\underline{\lambda}(M)$). The maximum (minimum) of a finite set of real values γ_k, $k = 1,2,\ldots,N$, denoted as $\max(\gamma_k)$ ($\min(\gamma_k)$).

3.3 Problem formulation

Consider N identical agents modeled as Linear Time-Invariant (LTI) systems

$$\begin{aligned} \dot{x}_i &= A_a x_i + u_{c_i} + B_a u_i \\ y_i &= C_a x_i \\ y_{c_i} &= x_i, \end{aligned} \tag{3.1}$$

$$u_{c_i} = \sum_{j=1}^{N} l_{c_{ij}} A_c y_{c_j} \tag{3.2}$$

where $A_a \in \mathbb{R}^{n\times n}$, $B_a \in \mathbb{R}^{n\times m}$, $C_a \in \mathbb{R}^{p\times n}$; $x_i \in \mathbb{R}^n$ is the state vector of agent i, $u_{c_i} \in \mathbb{R}^n$ is the *inherent coupling* of the ith agent to the remainder of the system, $u_i \in \mathbb{R}^m$ is the *control input* of the ith agent $y_{c_i} \in \mathbb{R}^n$ is the *coupling output* of the ith agent and $y_i \in \mathbb{R}^p$ is its *measured output*. Global inherent coupling topology is described by the *outer coupling matrix* $L_c = [l_{c_{ij}}]$, where the scalar $l_{c_{ij}}$ weights the *inner coupling matrix* $A_c \in \mathbb{R}^{n\times n}$ connecting agent j to agent i

$$u_c = (L_c \otimes A_c) y_c \tag{3.3}$$

This models inherent couplings usually found in LSS models, [4]. The major difference from conventional cooperative multi-agent dynamics are the additional terms $(L_c \otimes A_c)x$. Namely, we assume that agents are inherently coupled, regardless of applied controls. This structure is commonly found in distributed parameter systems, where high-order dynamics leads to couplings between subsystems chosen to partition the truncation of the original system.

The total coupled multi-agent system is then

$$\begin{aligned} \dot{x} &= (I_N \otimes A_a + L_c \otimes A_c)x + (I_N \otimes B_a)u \\ y &= (I_N \otimes C_a)x, \end{aligned} \tag{3.4}$$

where $x = [x_1^T, ..., x_N^T]^T$, $u = [u_1^T, ..., u_N^T]^T$, $y = [y_1^T, ..., y_N^T]^T$ are the total state, input and output vectors, respectively. We make the following assumption on the global interconnection topology.

Assumption 1 *The outer coupling matrix L_c is symmetric.*

The goal of this paper is to design single-agent control inputs u_i to stabi-

lize the state of the total system (4.13) to its origin.

For that purpose we make the following assumption.

Assumption 2 *The pair (A_a, B_a) is stabilizable.*

We further consider decentralized static state-feedback

$$u_i = pK_a x_i, \tag{3.5}$$

where $p > 0$ is a scalar control weight and $K_a \in \mathbb{R}^{m \times n}$ is a static state-feedback gain matrix. The overall closed-loop system is then given as

$$\begin{aligned} \dot{x} &= (I_N \otimes A_a + L_c \otimes A_c)x + (pI_N \otimes B_a K_a)x \\ y &= (I_N \otimes C_a)x. \end{aligned} \tag{3.6}$$

Remark 1 *In Assumption 1 the outer coupling matrix L_c is considered to be symmetric. Symmetric couplings occur in physical systems wherever the Laplacian operator appears in the infinite-dimensional partial differential equation (PDE) description: flexible structures, heat transfer, chemical diffusion, diffusion-reaction systems, acoustic fields,* etc.

3.4 Decentralized control design for systems with inherent couplings

This section brings a stabilization condition for closed-loop system (4.16), assuming the global inherent coupling matrix L_c satisfies Assumption 1. Furthermore, we design a decentralized state-feedback (4.15) to stabilize system (4.13) to its origin.

Some technical results familiar from the literature are introduced first.

Lemma 1 *[27] The LTI system $\dot{x} = Ax + Bu$ is stabilized via linear state-*

feedback $u = Kx$ if and only if there exists a $P > 0$ such that

$$(A+BK)^T P + P(A+BK) < 0. \tag{3.7}$$

Equivalently, if and only if there exists a $Q > 0$ such that

$$AQ + QA^T + BY + Y^T B^T < 0, \tag{3.8}$$

where $Y = KQ$.

Choosing the feedback gain K in Y as $K = -\frac{1}{2}B^T Q^{-1}$ brings an alternative stability condition

$$AQ + QA^T - BB^T < 0, \tag{3.9}$$

reducing the number of variables by one.

Therefore, any $Q > 0$ satisfying (4.19), provides a stabilizing state-feedback gain $K = -\frac{1}{2}B^T Q^{-1}$. ■

Note that the last part of Lemma 4 brings a specific stabilizing control design, not only a stabilizability condition.

Lemma 2 *The following Lemma is often used in distributed control literature, [28, 12] Let M be a block symmetric matrix of the form*

$$M = I_N \otimes M_D + L \otimes M_O, \tag{3.10}$$

where $M_D \in \mathbb{R}^{n\times n}$, $M_O \in \mathbb{R}^{n\times n}$, $L \in \mathbb{R}^{N\times N}$ are symmetric matrices and L is diagonalizable. Then M has eigenvalues

$$\lambda(M) = \lambda\left(M_D + \lambda_k(L) M_O\right). \tag{3.11}$$

Proof: *L is diagonalizable, i.e. there exists a transformation matrix T such that $TLT^{-1} = \Lambda$, where Λ is a diagonal matrix of eigenvalues of L.*

Choosing transformation matrix $T_M = T \otimes I_n$ therefore transforms M into $\hat{M} = T_M M T_M^{-1}$, where

$$\begin{aligned}\hat{M} &= (T \otimes I_n)(I_N \otimes M_D + L \otimes M_O)(T^{-1} \otimes I_n) \\ &= I_N \otimes M_D + \Lambda \otimes M_O\end{aligned} \tag{3.12}$$

is block-diagonal. As $\lambda(M) = \lambda(\hat{M})$, the latter eigenvalues being the eigenvalues of diagonal blocks $M_D + \Lambda_{kk} M_O$, this completes the proof. ■

Theorem 1 *Let the outer coupling matrix L_c satisfy Assumption 1. Let there exist a $Q_a > 0$ and $p > 0$ satisfying*

$$\begin{aligned}&\frac{1}{p}(A_a Q_a + Q_a A_a^T - p B_a B_a^T) + \overline{\lambda}(L_c)(A_c Q_a + Q_a A_c^T) < 0, \\ &\frac{1}{p}(A_a Q_a + Q_a A_a^T - p B_a B_a^T) + \underline{\lambda}(L_c)(A_c Q_a + Q_a A_c^T) < 0.\end{aligned} \tag{3.13}$$

Then the decentralized linear state-feedback (4.15) with the feedback gain

$$K_a = -\frac{1}{2} B_a^T Q_a^{-1}, \tag{3.14}$$

stabilizes the LTI system (4.13). Furthermore, feasibility of (4.21) is implied if the decentralized feedback K_a stabilizes (A_a, B_a).

Proof: *The stability criterion in Lemma 4 applied to system (4.13) requires*

$$\begin{aligned}&(I_N \otimes A_a + L_c \otimes A_c) Q + Q (I_N \otimes A_a + L_c \otimes A_c)^T \\ &- (I_N \otimes B_a)(I_N \otimes B_a)^T,\end{aligned} \tag{3.15}$$

to be a negative definite matrix for some positive definite $Q = Q^T \in \mathbb{R}^{n \cdot N \times n \cdot N}$.

The state-feedback implied by Lemma 4 is then given by

$$K = -\frac{1}{2}(I_N \otimes B_a)^T Q^{-1}, \tag{3.16}$$

Let the matrix Q be chosen as

$$Q = \frac{1}{p} I_N \otimes Q_a, \tag{3.17}$$

then the state-feedback (4.24) is in decentralized form

$$K = pI_N \otimes K_a, \tag{3.18}$$

where K_a is the local state-feedback gain matrix (4.22); $K_a = -1/2 B_a^T Q_a^{-1}$. The choice of Q in (4.25), renders the matrix (3.15) in the form

$$\begin{aligned}
&(I_N \otimes A_a + L_c \otimes A_c)(\frac{1}{p} I_N \otimes Q_a) \\
&+ (\frac{1}{p} I_N \otimes Q_a)(I_N \otimes A_a + L_c \otimes A_c)^T \\
&- (I_N \otimes B_a)(I_N \otimes B_a)^T \\
=&\frac{1}{p} I_N \otimes A_a Q_a + \frac{1}{p} L_c \otimes A_c Q_a + \frac{1}{p} I_N \otimes Q_a A_a^T \\
&+ \frac{1}{p} L_c^T \otimes Q_a A_c^T - I_N \otimes B_a B_a^T \\
=&\frac{1}{p}[I_N \otimes (A_a Q_a + Q_a A_a^T - p B_a B_a^T) \\
&+ L_c \otimes (A_c Q_a + Q_a A_c^T)].
\end{aligned} \tag{3.19}$$

With $A_D := \frac{1}{p}(A_a Q_a + Q_a A_a^T - p B_a B_a^T)$ and $A_O := A_c Q_a + Q_a A_c^T$, the matrix (4.27) can be concisely written as $I_N \otimes A_D + L_c \otimes A_O$. Since A_D, A_O and L_c are symmetric, the matrix (4.27) is symmetric and hence has only real eigenvalues. Therefore, (4.27) is negative definite if and only if all its eigenvalues

are negative.

Based on Lemma 2, the eigenvalues of (4.27) are the same as the eigenvalues of the matrices

$$\frac{1}{p}(A_aQ_a + Q_aA_a^T - pB_aB_a^T) + \lambda_k(L_c)(A_cQ_a + Q_aA_c^T), \tag{3.20}$$

for $k = 1,...,N$. Therefore, negative definiteness of (4.27) is equivalent to negative definiteness of the symmetric matrices (3.20) for all $k = 1,...,N$. The matrices $A_D + \gamma_k A_O = \frac{1}{p}(A_aQ_a + Q_aA_a^T - pB_aB_a^T) + \gamma_k(A_cQ_a + Q_aA_c^T)$, for $\gamma_k \in \mathbb{R}$, $k = 1,\ldots,N$, with generally indefinite $A_O = A_cQ_a + Q_aA_c^T$, are certainly negative definite for all γ_k if $A_D + \min(\gamma_k)A_O$ and $A_D + \max(\gamma_k)A_O$ are negative definite. Hence, (4.21) is sufficient for negative definiteness of all matrices (3.20), which guarantees stability of LTI system (4.13) with decentralized feedback (4.15), thus completing the proof. ■

Remark 2 *The choice of Q in (4.25) is commensurate with the multi-agent system structure, ultimately yielding decentralized control. Theorem 1 thus decouples the distributed nature of the system for decentralized controller design and allows feasible control design even for systems with a large number of agents. This is in contrast to [19] and [18], which consider the entire system model for decentralized control design.*

3.4.1 Recurrent outer coupling matrix

The couplings between agents are identical, described by the inner coupling matrix A_c. In our specific case, the corresponding physical interconnection

topology is globally described by the outer coupling matrix L_c,

$$L_c = \begin{bmatrix} \alpha & \beta & & \\ \beta & \ddots & \ddots & \\ & \ddots & \alpha & \beta \\ & & \beta & \alpha \end{bmatrix}, \tag{3.21}$$

which has a recurrent structure. That is, we take that agent k is inherently coupled with agent $k-1$ and agent $k+1$ for $k = 2 \ldots N-1$, while the first and the last agent are coupled only with the second and $N-1$st, respectively. Now we have the following result.

Lemma 3 *[29] The eigenvalues of the tridiagonal matrix (3.21) are*

$$\lambda_k(L_c) = \alpha + 2\beta \cos \frac{k\pi}{N+1}, \quad k = 1, 2, \ldots, N. \tag{3.22}$$

■

From now on we furthermore assume that $\alpha = 0$, $\beta = 1$.

Corollary 1 *Let the conditions of Theorem 1 be satisfied. Let the matrix L_c be in the form (3.21) with $\alpha = 0$, $\beta = 1$. Then condition (4.21) becomes*

$$\frac{1}{p}(A_a Q_a + Q_a A_a^T - p B_a B_a^T) \pm \gamma_1 (A_c Q_a + Q_a A_c^T) < 0, \tag{3.23}$$

where $\gamma_1 = 2\cos\left(\frac{\pi}{N+1}\right)$.

Proof: *Based on the above assumptions, the matrix (4.27) is block tridiagonal, with symmetric diagonal blocks* $A_D = \frac{1}{p}(A_aQ_a + Q_aA_a^T - pB_aB_a^T)$, *and symmetric blocks* $A_O = A_cQ_a + Q_aA_c^T$. *By Lemma 2 applied to (4.27) and Lemma 3 applied to* L_c *(3.21) with* $\alpha = 0$, $\beta = 1$, *the eigenvalues of (4.27),* $\lambda\left(I_N \otimes A_D + L_c \otimes A_O\right)$, *are*

$$\begin{aligned} &\lambda\left(A_D + \gamma_k A_O\right), \\ &\gamma_k = 2\cos\left(\frac{\pi k}{N+1}\right), \quad k = 1,\ldots,N. \end{aligned} \tag{3.24}$$

For any N, $\max(\gamma_k) = \gamma_1 = -\gamma_N = -\min(\gamma_k)$. *Then Theorem 1 concludes the proof.* ■

Remark 3 *Condition (3.23) depends on the number of agents, (i.e. the size of the system), only through the constant* γ_1. *The limit case where the number of agents tends to infinity implies the strictest bound for (3.23) with* $\gamma_1 = 2$. *Thus, the linear state-feedback gain (4.22) stabilizes system (4.16) for any number of agents if condition (3.23) is met with* $\gamma_1 = 2$.

For practical application of our main result, we formulate the design condition (3.23) as a set of LMIs

Algorithm 1

1. $\frac{1}{p}(A_aQ_a + Q_aA_a^T - pB_aB_a^T) + \gamma_1(A_cQ_a + Q_aA_c^T) < 0$,
2. $\frac{1}{p}(A_aQ_a + Q_aA_a^T - pB_aB_a^T) - \gamma_1(A_cQ_a + Q_aA_c^T) < 0$,
3. $-Q_a < 0$,

which is efficiently solvable using standard tools such as MATLAB, CVX, MOSEK, etc. After solving the LMIs one obtains both the solution Q_a *and the scalar gain p for which the LMIs are solvable. The local state-feedback*

gain K_a is then computed and applied to every agent, thus stabilizing the entire system.

Remark 4 *After running Algorithm 1, the scalar gain p can be modified to adjust how aggressive the controller is, as long as condition (3.23) still holds. Namely, the larger the value of p, the more aggressive the controller and vice-versa.*

3.5 Numerical example

The proposed control design is presented on a numerical model of a smart flexible structure [30], [31]. The model of a flexible beam with two degrees of freedom and N actuators is used. Each actuator is modeled as a second-order dynamical system. By an appropriate arrangement of state variables in the system model, we obtain a dynamical system in the form (4.13) with single-agent dynamics $A_a \in \mathbb{R}^{6\times 6}$ and inner coupling matrix $A_c = \mathbb{R}^{6\times 6}$. Each agent has one control input. The topology of underlying inherent interconnections between the agents is described by the outer coupling matrix $L_c \in \mathbb{R}^{N\times N}$ (3.21) with $\alpha = 0, \beta = 1$, satisfying Assumption 1.

$$A_a = \begin{bmatrix} 0 & 32 & 0 & 0 & 0 & 0 \\ -93.8 & -0.110 & 0 & 0 & 0 & 0 \\ 0 & 0 & 0 & 0 & 512 & 0 \\ 0 & 0 & 0 & 0 & 0 & 2048 \\ 0 & 179.5 & -831 & 0 & -43.5 & 0 \\ 0 & 0 & 0 & -1953 & 0 & -401 \end{bmatrix},$$

$$A_c = \begin{bmatrix} 0 & 0 & 0 & 0 & 0 & 0 \\ 0 & 0 & 0 & 0 & 0 & 0 \\ 0 & 0 & 0 & 0 & 0 & 0 \\ 0 & 0 & 0 & 0 & 0 & 0 \\ 0 & 0 & -415.48 & 0 & -21.1 & 0 \\ 0 & 0 & 0 & -976.563 & 0 & -199.75 \end{bmatrix}, \tag{3.25}$$

$$B_a = \begin{bmatrix} 0 & 0.7324 & 0 & 0 & 0 & 0 \end{bmatrix}^T$$

Flexible structure with $N = 10$ and $N = 100$ nodes is first shown damped by two existing control design approaches whose performance is compared with that of the presented design. The first control design approach is representative of optimization methods using the entire system model for controller synthesis based on LMIs, such as in e.g. [18]. The second control design is a classical Linear Quadratic Regulator (LQR), using the entire system model. Finally, the performance of a decentralized controller based on Theorem 1 is presented. The solution of LMIs based on condition (3.23) is found with MOSEK solver.

3.5.1 Structure with 10 nodes

Bode magnitude plots of the uncontrolled system and the system controlled by three different controllers are shown compared in Figure 3.1. This figure

only illustrates three possible approaches applicable in this case with a low number of agents corresponding to the system-order 60. Of course, different controller tuning leads to different closed-loop (CL) frequency characteristics.

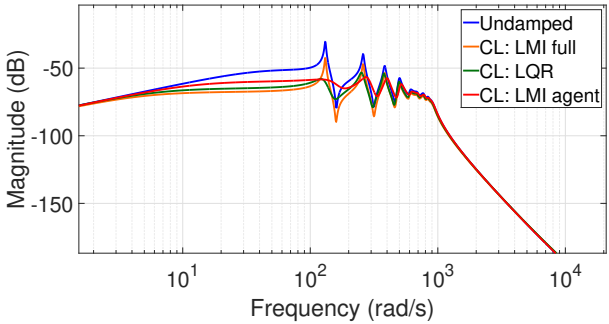

Figure 3.1: Bode magnitude plots of the undamped flexible structure and flexible structure with three different controllers. Input is the first node's vertical displacement, and output is the vertical displacement of the second node. The structure has 10 nodes,the order of the system is 60.

3.5.2 Structure with 100 nodes

A more reasonable example of our approach is provided by control design for larger systems where other methods fail or give centralized controllers without specific structure. A flexible structure with 100 nodes is used in this case. Even for this system of order 600, the first approach using the full design model and LMI formulation fails. Closed-loop Bode magnitude plots with an LQR controller and decentralized state-feedback design based on single-agent dynamics and coupling matrix are depicted in Figure 3.2. Both results yield similar frequency characteristics. However, the decentralized controller has a much simpler recurrent structure with $K = pI_N \otimes K_a$ compared to the

LQR leading to the full, non-sparse, matrix gain K with many non-zero entries.

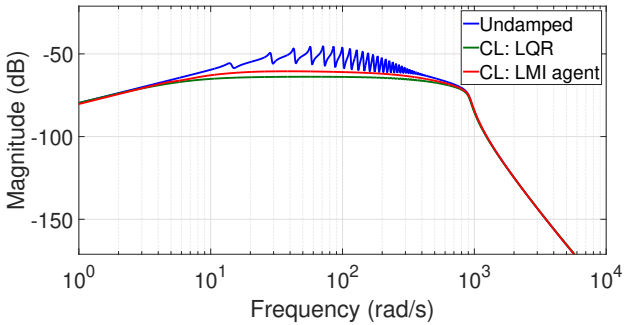

Figure 3.2: Bode magnitude plots of the undamped flexible structure and the flexible structure with LQR and decentralized state-feedback. Input is the vertical displacement of the first node, and the output is the vertical displacement of the second node. The structure has 100 nodes so the order of the system is 600.

Decentralized state-feedback is given by (4.22) and scalar gain p. The solution obtained from MOSEK or other numerical solvers could damp the system too much, with control action exceeding the maximum allowed value. The gain p can then be used for final controller tuning. Three different choices for gains: high p_1, medium p_2, and low p_3 are presented in Figures 3.3, 3.4, and 3.5. Damping of the resulting closed-loop system can be easily controlled with the scalar gain p, which is another benefit of our method.

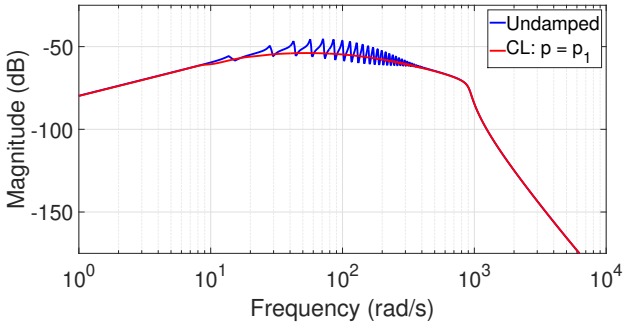

Figure 3.3: Bode magnitude plots of the undamped flexible structure and flexible structure with decentralized state-feedback having $p = p_1$. Input is the vertical displacement of the first node, and the output is the vertical displacement of the second node. The structure has 100 nodes so the order of the system is 600.

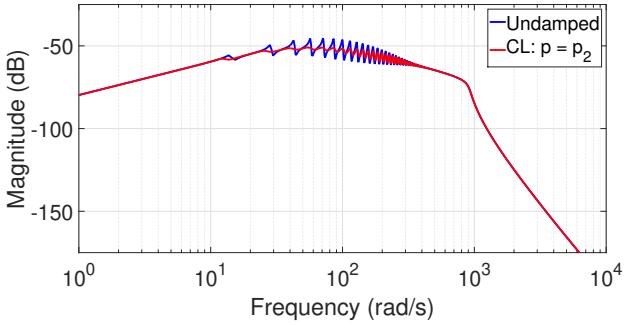

Figure 3.4: Bode magnitude plots of the undamped flexible structure and flexible structure with decentralized state-feedback having $p = p_2$. Input is the vertical displacement of the first node, and the output is the vertical displacement of the second node. The structure has 100 nodes so the order of the system is 600.

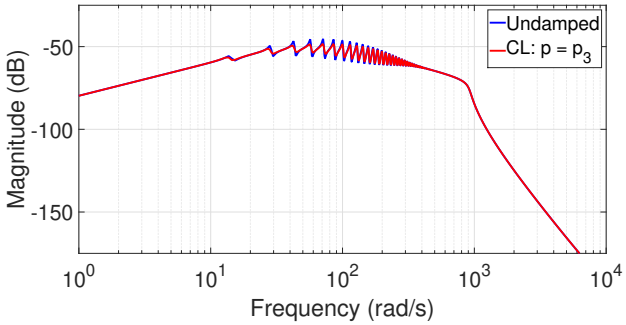

Figure 3.5: Bode magnitude plots of the undamped flexible structure and flexible structure with decentralized state-feedback having $p = p_3$. Input is the vertical displacement of the first node, and the output is the vertical displacement of the second node. The structure has 100 nodes so the order of the system is 600.

3.6 Conclusions

In this paper, we present a simple design of stabilizing decentralized state-feedback for LSS, based on single-agent dynamics. The considered model is usually found in flexible structures involving inherent connections to neighboring agents forming a recurrent pattern. Based on the closed-loop stability condition, LMIs are derived guaranteeing stabilizing state-feedback. Crucially, the dimension of the derived LMIs remains the same with growing number of agents; the design thus remains feasible even for large complex systems. A numerical example of a smart flexible structure is given. The presented approach outperforms existing control designs based on the model of the entire system. Generalization to distributed control is the subject of future work.

References

[1] S. Xu, J. Bao, Distributed control of plantwide chemical processes, Journal of Process Control 19 (2009) 1671–1687. doi:10.1016/j.jprocont.2009.07.007.

[2] A. Emami-Naeini, J. Ebert, D. de Roover, R. Kosut, M. Dettori, L. Porter, S. Ghosal, Modeling and control of distributed thermal systems, IEEE Transactions on Control Systems Technology 11 (5) (2003) 668–683. doi:10.1109/TCST.2003.816411.

[3] S. Algermissen, T. Fröhlich, H. Monner, Hierarchical, decentralized control system for large-scale smart-structures, Smart Materials and Structures 23 (2014) 085037. doi:10.1088/0964-1726/23/8/085037.

[4] J. Mohammadpour Velni, K. Grigoriadis, Efficient Modeling and Control of Large-Scale Systems, 2010. doi:10.1007/978-1-4419-5757-3.

[5] M. Li, Z. Shuai, Global-stability problem for coupled systems of differential equations on networks, J. Differential Equations 248 (2010) 1–20. doi:10.1016/j.jde.2009.09.003.

[6] N. Sandell, P. Varaiya, M. Athans, M. Safonov, Survey of decentralized control methods for large scale systems, IEEE Transactions on Automatic Control 23 (2) (1978) 108–128. doi:10.1109/TAC.1978.1101704.

[7] P. Benner, Solving large-scale control problems, Control Systems, IEEE 24 (2004) 44 – 59. doi:10.1109/MCS.2004.1272745.

[8] W. Haddad, D. Bernstein, Combined l_2/h_∞ model reduction, International Journal of Control 49 (5) (1988) 1523–1535.

[9] A. Ilka, N. Murgovski, J. Sjöberg, An iterative newton's method for output-feedback lqr design for large-scale systems with guaranteed convergence, in: 2019 18th European Control Conference (ECC), 2019, pp. 4849–4854. doi:10.23919/ECC.2019.8795752.

[10] J. Lunze, Networked Control of Multi-Agent Systems, Bookmundo Direct, 2019.

[11] R. Olfati-Saber, J. A. Fax, R. M. Murray, Consensus and cooperation in networked multi-agent systems, Proceedings of the IEEE 95 (1) (2007) 215–233. doi:10.1109/JPROC.2006.887293.

[12] Z. Li, Z. Duan, G. Chen, L. Huang, Consensus of multiagent systems and synchronization of complex networks: A unified viewpoint, IEEE Transactions on Circuits and Systems I: Regular Papers 57 (1) (2010) 213–224. doi:10.1109/TCSI.2009.2023937.

[13] H. Zhang, F. L. Lewis, A. Das, Optimal design for synchronization of cooperative systems: State feedback, observer and output feedback, IEEE Transactions on Automatic Control 56 (8) (2011) 1948–1952. doi:10.1109/TAC.2011.2139510.

[14] Y. Hong, X. Wang, Z.-P. Jiang, Multi-agent coordination with general linear models: A distributed output regulation approach, in: IEEE ICCA 2010, 2010, pp. 137–142. doi:10.1109/ICCA.2010.5524157.

[15] K. H. Movric, F. L. Lewis, Cooperative optimal control for multi-agent systems on directed graph topologies, IEEE Transactions on Automatic Control 59 (3) (2014) 769–774. doi:10.1109/TAC.2013.2275670.

[16] J. Jiao, H. L. Trentelman, M. K. Camlibel, A suboptimality approach to distributed linear quadratic optimal control, IEEE Transactions on Automatic Control 65 (3) (2020) 1218–1225. doi:10.1109/TAC.2019.2923082.

[17] J. Schuppen, O. Boutin, P. Kempker, J. Komenda, T. Masopust, N. Pambakian, A. Ran, Control of distributed systems: Tutorial and overview, European Journal of Control 17 (2011) 579–602. doi:10.3166/EJC.17.579-602.

[18] R. D'Andrea, A linear matrix inequality approach to decentralized control of distributed parameter systems, in: Proceedings of the 1998 American Control Conference. ACC (IEEE Cat. No.98CH36207), Vol. 3, 1998, pp. 1350–1354 vol.3. doi:10.1109/ACC.1998.707015.

[19] Jankowski, B. Popławski, G. Mikułowski, A. Mróz, Decentralized semi-active damping of free structural vibrations by means of structural nodes with an on/off ability to transmit moments, Mechanical Systems and Signal Processing 100. doi:10.1016/j.ymssp.2017.08.012.

[20] Y.-X. Li, G.-H. Yang, Adaptive fuzzy decentralized control for a class of large-scale nonlinear systems with actuator faults and unknown dead zones, IEEE Transactions on Systems, Man, and Cybernetics: Systems 47 (5) (2017) 729–740. doi:10.1109/TSMC.2016.2521824.

[21] B. Labibi, B. Lohmann, A. Sedigh, P. Maralani, Decentralized stabilization of large-scale systems via state-feedback and using descriptor systems, IEEE Transactions on Systems, Man, and Cybernetics - Part A: Systems and Humans 33 (6) (2003) 771–776. doi:10.1109/TSMCA.2003.818463.

[22] N. Luo, J. Rodellar, M. De la Sen, J. Vehí, Decentralized active control of a class of uncertain cable-stayed flexible structure, Interna-

tional Journal of Control - INT J CONTR 75 (2002) 285–296. doi:10.1080/00207170110110559.

[23] P. Hušek, F. Svoboda, M. Hromčík, Z. Šika, Low-complexity decentralized active damping of one-dimensional structures, Shock and Vibration 2018 (2018) 1–9. doi:10.1155/2018/6421604.

[24] J. Xiang, Y. Li, D. Hill, Cooperative output regulation of multi-agent systems coupled by dynamic edges, IFAC Proceedings Volumes 47 (3) (2014) 1813–1818, 19th IFAC World Congress. doi:https://doi.org/10.3182/20140824-6-ZA-1003.02164.

[25] P. Massioni, M. Verhaegen, Distributed control for identical dynamically coupled systems: A decomposition approach, IEEE Transactions on Automatic Control 54 (1) (2009) 124–135. doi:10.1109/TAC.2008.2009574.

[26] Z. He, Y. Lu, Constrained cooperative control design for distributed morphing wing systems, Journal of Systems Engineering and Electronics 23 (4) (2012) 588–595. doi:10.1109/JSEE.2012.00073.

[27] S. Boyd, L. Ghaoui, E. Feron, V. Balakrishnan, Linear matrix inequalities in system and control theory, SIAM studies in applied mathematics 24.

[28] G. Lafferriere, A. Williams, J. Caughman, J. Veerman, Decentralized control of vehicle formations, Systems Control Letters 54 (2005) 899–910. doi:10.1016/j.sysconle.2005.02.004.

[29] J. Elliott, The characteristic roots of certain real symmetric matrices, Master's thesis, Univ. of Tennessee, USA, 1953.

[30] T. Tao, K. D. Frampton, Experiments on distributed active vibration control of a simply supported beam, Smart Materials and Structures

15 (6) (2006) 1858. doi:10.1088/0964-1726/15/6/040.
URL https://dx.doi.org/10.1088/0964-1726/15/6/040

[31] F. Svoboda, M. Hromčík, Finite element method based modeling of a flexible wing structure, in: 21st International Conference on Process Control, Strbske Pleso, Slovakia, IEEE, 2017. doi:10.1109/PC.2017.7976217.

4. Decentralized active damping control for aeroelastic morphing wing

This paper introduces a novel decentralized control design procedure for an aeroelastic morphing wing. The control goal is active damping of this flexible system. The model is developed as a multi-agent system with inherent interconnections between the agents. The control system then takes advantage of the model structure and interconnections rather than relying on the entire system's model. This brings benefits, especially with a growing number of agents where the control design dimension remains low. Therefore, the proposed control design is especially suitable for morphing wings with a large number of actuation points. The result is presented in the Linear Matrix Inequalities (LMIs) form. A numerical example shows the application of the proposed algorithm.

This chapter was published in:
F. Svoboda, K. Hengster-Movric, M. Hromčík, Z. Šika, Decentralized active damping control for aeroelastic morphing wing, Aerospace Science and Technology 139 (2023) 108415. doi:10.1016/j.ast.2023.108415.

4.1 Introduction

Aerodynamic morphing bodies such as morphing wind power generator blades or morphing wings are a promising trend with potential high efficiency. However, a variable airfoil geometry is also challenging for control due to aeroelastic phenomena that must be considered. One elegant solution for such flexible wing constructions is furnished by active damping, avoiding undesirable vibrations or even flutter [1], [2].

In the last twenty years, smart materials developments accelerated research of morphing wing concepts [3, 4]. This new promising technology works with the idea of changing the wing profile geometry, enabling a mission-adaptive performance and effective active damping of aeroelastic modes [5]. Current conventional wings are usually designed for either a single cruise flight condition or a weighted combination of multiple flight conditions. They are thus not optimal for a wide range of flight modes. Continuously variable profile geometries promise significantly increased efficiency, minimized drag, and low noise levels compared to wings with conventional flaps. Furthermore, the use of smart materials eliminates the need for large and heavy traditional actuators. Related weight and drag reductions directly translate into significant fuel savings and operating cost reduction.

Several research groups, often in collaboration with NASA, have already shown their technical solutions of aerodynamic morphing structures [6]. For example, the Variable Camber Continuous Trailing Edge Flap (VCCTEF) design, developed under the NASA Performance Adaptive Aeroelastic Wing (PAAW) project, includes 17 flaps that can be individually controlled [7]. The segments are joined by a flexible and supporting material, thus providing continuous flaps throughout the wingspan with no drag producing gaps. A lightweight Shape Memory Alloys (SMA) solution is proposed in [8]. The difference between the weight of an SMA actuator and an electric motor ac-

tuator can be significant and plays a substantial role in increasing efficiency [9]. Morphing leading and trailing edge with composite skin was developed and tested in [10]. A subscale plane model with morphing wings and a smart actuation system has been developed at ETH Zurich [11]. ETH's construction is based on optimized compliant ribs, corrugated skin, and Macro Fiber Composite (MFC) piezoelectric elements for actuation. Another morphing wing construction was presented by MIT [12] employing a modular approach with low density and highly compliant structures. The Delft University of Technology presented its variable chord length and camber concept [13], where the range of flight missions can be extended more effectively by changing the wing characteristics. The benefits of morphing trailing edge technology are also studied by the University of Michigan research team [14]. In this research, a high fidelity model with hundreds of variables shows a potential cruise fuel reduction of over 5% with morphing trailing edge along the aft 40% of the wing. Bioinspired control of morphing wing with Macro Fiber Composite actuators is also studied at the University of Michigan [15]. Bioinspired discrete wing structure is also presented in [16]. Authors in [17] use an active tensegrity structure concept with pneumatic actuators and latex skin. Their prototype was tested in a wind tunnel. Wind tunnel test and high-lift morphing wing performance were also presented in [18].

Since the morphing wing technology currently appears feasible and promising for near-future wind power generation and air transportation systems, control design methodologies for such systems are in high demand. Lightweight and highly flexible aerodynamic structures [19], [20], [21] bring the necessity of suppressing the undesirable aeroelastic effects such as flutter. Furthermore, the high number of actuators and the increased complexity of the system present a challenge for the control design. Cooperative control, however, provides opportunities to decompose the original problem into simpler, more tractable parts.

Cooperative control conventionally deals with distributed protocols and agent-based dynamical models. Studied systems consist of autonomous subsystems, called *agents* [22], each of which addresses, in a coordinated manner, a specific sub-task to attain the overall design objective. Cooperative control is currently a very active field of research, thanks to potential applications that require high scalability and reliability. A cooperative multi-agent system is commonly described by a graph, with nodes representing dynamical subsystems and edges representing interactions between them, [23]. The extensively researched canonical problems in cooperative control of multi-agent systems are *consensus* and *synchronization*, [24]. However, those are typically studied for systems without any inherent interactions between the subsystems; the controller alone ensuring agent interactions, as usually found in mobile robot formations, multi-vehicle systems, etc. The applied control laws in those cases thus form a distributed virtual connection between the originally uncoupled agents. In particular, [25] proposes a framework for synchronizing cooperative systems via full state-feedback. This allows designing stabilizing cooperative state-feedback controllers based only on single-agent dynamics and the pertaining local algebraic Riccati equation. Synchronization using dynamic compensators or output-feedback is presented in [24, 26]. Furthermore, [27] considers the optimality of cooperative control protocols concerning a global quadratic performance criterion.

Nevertheless, multi-agent systems in conventional cooperative control theory consider inherently independent single-agent dynamics, where the connection between agents is made through control law. Unfortunately, these cooperative control results do not extend straightforwardly to systems having inherent interconnections between subsystems. One such system that could be described as a multi-agent system with inherent couplings is the morphing aeroelastic wing. Morphing aeroelastic wing has distributed local subdynamics inseparably connected with neighboring subdynamics through mechanical

couplings.

On the other hand, there are various methods of dealing with distributed control design. For instance, the work [28] studies a flexible beam model with bending and torsion motions and a distributed control arrangement with two force-actuators and three torque-actuators paired with rate gyros. Aeroservoelastic design of piezo-composite wing is also presented in [29]. In [30], a dense network of piezoelectric patch actuators was proposed to realize the distributed actuation. In [31], a distributed piezoelectric actuation is involved and applied to patches' placement problem to suppress the deformations at pre-selected locations. Since the flexible systems are passive by nature, one can employ many results available for distributed control of passive systems [32]. Completely passive solutions based on piezo-structures are reported in [33]. However, these methods require the whole system model for design, and those could turn out to be infeasible for highly complex systems, same as centralized control designs. In particular, [34] brings an LMI approach to decentralized control design for distributed parameter systems having a specific structure. However, that result is generally conservative, and it relies on the entire system model. Similarly, [35], [36] also presents decentralized control design with a model of the entire system. For large systems (having many agents), using the entire system model for control design often leads to computationally infeasible solutions. In contrast, [37] considers the detailed structure of a multi-agent system with inherently coupled agents for control design, providing decentralized state-feedback to minimize the effects of subsystem interactions and guarantee the stability of the whole system. Despite using the system structure, the method proposed in [37] is found to be conservative, scaling rather unfavorably with a growing number of agents. In [38] and [39] a flexible structure is decomposed into N coupled subsystems, and decentralized control of one-dimensional subsystems is subsequently examined. Both latter approaches only consider one-dimensional structures,

which ultimately limits their applicability. The special structure of the coupled multi-agent systems is also assumed in [40], where a passive dynamical system interconnects the agents. This interconnection contains integrators, so a direct connection between agents' states is not considered. A computationally favorable control design methodology for systems with inherently directly coupled subsystems based on single-agent dynamics akin to that found in cooperative control theory is, thus, still lacking.

Our novel control design strategy is based on cooperative control ideas to ensure good scalability and feasibility, even for highly complex systems. This method benefits from the sparsity of agent interactions modeled by a network. Instead of relying on the whole system model, our method relies on the smaller model of its recurring parts.

The remainder of this paper is organized as follows. The notation and the considered aeroelastic wing model are provided in Section 2. Section 3. presents the problem formulation. The main result is covered in Section 4. We present an LMI relaxation procedure in Section 5. A simulation case study is presented in Section 6, with emphasis on numerical experiments and system analysis. Finally, conclusions are drawn in Section 7.

4.2 Preliminaries

Notations: $I_N \in \mathbb{R}^{N\times N}$ is the identity matrix. Kronecker product is denoted by $\otimes$. $L = [l_{ij}]$ is a matrix with entry l_{ij} in ith row and jth column. $D = \text{diag}\{d_i\}$ is a diagonal matrix with diagonal entries d_i. Matrix $Q > 0$ ($Q < 0$) is positive (negative) definite. $\lambda(M)$ are eigenvalues of a matrix M. The maximum (minimum) eigenvalues are denoted by $\overline{\lambda}(M)$ ($\underline{\lambda}(M)$). The maximum (minimum) singular value is denoted by $\overline{\sigma}(M)$ ($\underline{\sigma}(M)$). We use notation where $\mu(\cdot)$ is matrix measure associated with matrix norm $\|\cdot\|$.

In this paper, various distributed and decentralized control approaches are

discussed. Let us emphasize from the outset that these terms, although used synonymously in some texts, actually describe two distinct approaches. A decentralized controller consists of local independent controllers for individual parts of the plant (agents). If local controllers also share information with their neighbors, then we talk about distributed control.

A model of the aeroelastic morphing wing is developed for control design. This model assumes a *rectangular wing* with a *morphing trailing edge*. Deformation of the trailing edge is ensured by distributed actuators (for example, servomechanism or smart materials). In general, the aeroelastic wing model consists of a structural part, an aerodynamic part, and actuators. In this paper, the *strip-theory* approach is used for aeroservoelastic model development [7]. The aeroelastic wing is modeled as an Euler-Bernoulli beam with the aerodynamic loads acting on the wing represented by Theodorsen's unsteady aerodynamics [41] and second-order systems as actuators. Similar models are widely used in the literature [42, 43, 44]. Structural and aerodynamic modeling are also discussed in [45] where some other methods are presented, such as simple two degrees of freedom or high fidelity models.

Finite Element Methods (FEMs) are common in aircraft aeroelastic calculations; those approximate the behavior of the continuous mechanical structure. FEM methods divide the structure into a number of elements of finite dimension interconnected at discrete points. In this work, each finite element itself is modeled as an Euler-Bernoulli beam with three degrees of freedom. Euler-Bernoulli beam theory considers small displacements and linear elastic material, therefore the Hook law is valid. Euler-Bernoulli beam with transverse displacement u, elastic modulus E and second moment of area I is described by equation (4.1).

$$EI\frac{d^4u}{dx^4} = -f \tag{4.1}$$

The solution of equation (4.1) with boundary conditions can be formulated

with mass (4.3) and stiffness (4.2) matrices for one beam element (Figure 4.1), where m_l is mass per unit length, j_l is inertia per unit length, G is modulus of rigidity, I_z is moment of area and l is a length of a beam. Columns in the matrixes correspond to vector $x_e = \begin{bmatrix} h_{i-1} & \theta_{i-1} & \phi_{i-1} & h_i & \theta_i & \phi_i \end{bmatrix}^T$.

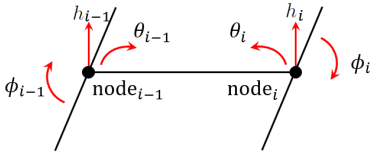

Figure 4.1: The Euler-Bernoulli beam emlemt with three degrees of freedom.

$$k_e = \begin{bmatrix} \frac{12EI_z}{l^3} & \frac{6EI_z}{l^3} & 0 & \frac{-12EI_z}{l^3} & \frac{6EI_z}{l^2} & 0 \\ \frac{6EI_z}{l^2} & \frac{4EI_z}{l} & 0 & \frac{-6EI_z}{l^2} & \frac{2EI_z}{l} & 0 \\ 0 & 0 & \frac{GJ_x}{l} & 0 & 0 & \frac{-GJ_x}{l} \\ \frac{-12EI_z}{l^3} & \frac{-6EI_z}{l^3} & 0 & \frac{12EI_z}{l^3} & \frac{-6EI_z}{l^2} & 0 \\ \frac{6EI_z}{l^2} & \frac{2EI_z}{l} & 0 & \frac{-6EI_z}{l^2} & \frac{4EI_z}{l} & 0 \\ 0 & 0 & \frac{-GJ_x}{l} & 0 & 0 & \frac{GJ_x}{l} \end{bmatrix} \tag{4.2}$$

$$m_e = \begin{bmatrix} \frac{156m_l l}{420} & \frac{22m_l l^2}{420} & 0 & \frac{54m_l l}{420} & \frac{-13m_l l^2}{420} & 0 \\ \frac{22m_l l^2}{420} & \frac{4m_l l^3}{420} & 0 & \frac{13m_l l^2}{420} & \frac{3m_l l^3}{420} & 0 \\ 0 & 0 & \frac{j_l l}{3} & 0 & 0 & \frac{j_l l}{6} \\ \frac{54m_l l}{420} & \frac{13m_l l^2}{420} & 0 & \frac{156m_l l}{420} & \frac{-22m_l l^2}{420} & 0 \\ \frac{-13m_l l^2}{420} & \frac{-3m_l l^3}{420} & 0 & \frac{-22m_l l^2}{420} & \frac{4m_l l^3}{420} & 0 \\ 0 & 0 & \frac{j_l l}{6} & 0 & 0 & \frac{j_l l}{3} \end{bmatrix} \tag{4.3}$$

By joining individual Euler-Benouli elements, we get the final elastic structure and equation of motion (4.4). Damping matrix C_S was derived as Rayleigh damping, i.e., a linear combination of the mass and stiffness matrices $C_s =$

$a_0 M_s + a_1 K_s$.

$$M_s \ddot{X}_s + C_s \dot{X}_s + K_s X_s = F_s, \tag{4.4}$$

Matrices M_s, C_s and K_s are the wing mass, damping and stiffness matrices of the whole structure, F_s is a generalized force vector (forces and torques). Vector X_s contains displacement variables of each node. More details about FEM elastic wing structure modeling can be found in [46]. Generalized force vector F_s from equation (4.4) consists of aerodynamic forces and torques. In this model, Theodorsen's unsteady aerodynamics is considered. The aerodynamic lift L_i and torque M_{α_i} can be found in [41]. Equations (4.5) are based on *potential flow*, where Theodorsens function $C(k)$, with $k = \frac{\omega b}{V}$, the reduced frequency depending on angular frequency ω, wing semi-chord b and airspeed V, models the unsteady behavior of a wing section. Constants T_p with $p = 1,4,5,7,10,11,12$ are associated with the integration of velocity potentials [41], a is nondimensional distance from midchord to axis of rotation (elastic axis), c is nondimensional distance from midchord to morphing trailing edge hinge, and ρ is an air density.

$$\begin{aligned}
L_i =& -\rho b^2 l\left(V\pi\dot{\alpha}_i + \pi\ddot{h}_i - \pi ba\ddot{\alpha}_i - VT_4\dot{\beta}_i - T_1 b\ddot{\beta}_i\right) \\
& - 2\pi\rho V blC(k)\left(V\alpha_i + \dot{h}_i + b\left(\frac{1}{2}-a\right)\dot{\alpha}_i + \frac{1}{\pi}T_{10}V\beta_i + b\frac{1}{2\pi}T_{11}\dot{\beta}_i\right) \\
M_{\alpha_i} =& -\rho b^2 l\left(-\pi ab\ddot{h}_i + \pi b^2\left(\frac{1}{8}+a^2\right)\ddot{\alpha}_i - b^2\left(T_7 + (c-a)T_1\right)\ddot{\beta}_i\right. \\
& + \pi bV\left(\frac{1}{2}-a\right)\dot{\alpha}_i + bV\left(T_1 - T_8 - (c-a)T_4 + \frac{1}{2}T_{11}\right)\dot{\beta}_i \\
& \left. + \left(T_4 + T_{10}\right)V^2\beta_i\right) + 2\pi\rho b^2 lV\left(\frac{1}{2}+a\right)C(k)\left(V\alpha_i + \dot{h}_i\right. \\
& \left. + b\left(\frac{1}{2}-a\right)\dot{\alpha}_i + \frac{1}{\pi}T_{10}V\beta_i + b\frac{1}{2\pi}T_{11}\dot{\beta}_i\right)
\end{aligned} \tag{4.5}$$

The morphing trailing-edge is modeled as a set of discrete flaps with a hinge in each wing segment i. The angle of this controlled trailing-edge of wing segment i is β_i. Trailing-edge actuation is ensured by servomechanism modeled as second-order systems (4.9). Angles β_i and their first and second derivatives are obtained from these systems.

Unsteady forces are represented in equations (4.5) as a circulatory terms occuring due to the vorticity in the flow and they are related to the Theodorsen function which reduces magnitude of the lift and an introduction of a phase lag between the airfoil motion and the unsteady fotrces. Theodorsen function $C(k)$ can be expressed in terms of Hankel functions $H_u = j_u - jY_u$, where J_u and Y_u are Bessel functions of the first and second kind. This expression is well-defined only for a simple harmonic motion of the airfoil. Therefore we use modified Bessel functions $K_u(jk)$, which are defined in the entire complex plane.

$$C(k) = \frac{H_1(k)}{H_1(k) + jH_0(k)} = \frac{K_1(jk)}{K_0(jk) + K_1(jk)}. \tag{4.6}$$

By using approximation from [45] we can model (4.6) by transfer function

$$C(s) = \frac{s^2 + 0.2804Vbs + 0.0135V^2}{b^2s^2 + 0.345Vbs + 0.0135V^2}. \tag{4.7}$$

After transforming (4.7) to controllable canonical form we get second order system 4.8.

$$\begin{aligned} \dot{z}_C &= \begin{bmatrix} -\frac{0.0345V}{b} & -\frac{0.0135V^2}{b^2} \\ 1 & 0 \end{bmatrix} z_C + \begin{bmatrix} 1 \\ 0 \end{bmatrix} u_C \\ y_C &= \begin{bmatrix} \frac{0.2804Vb - \frac{0.2804V - b}{b}}{b^2} & \frac{0.0135V^2 - \frac{0.0135V^2 - b^2}{b^2}}{b^2} \end{bmatrix} z_C + 0.5u_C \end{aligned} \tag{4.8}$$

Filters (4.8) are used for both circulatory terms in L_i, M_{α_i} and for all wing segments/agents, thus $z_C = \begin{bmatrix} \dot{z}_{\varepsilon_i} & z_{\varepsilon_i} \end{bmatrix}^T$, where $\varepsilon = h, \phi$.

Aerodynamic forces acting on the structural model are modified through trailing edge deformations. These deformations are due to the actions of controlled actuators.

The second-order system describes the actuator dynamics with a state-space model (4.9)

$$\begin{aligned}
\begin{bmatrix} \dot{x}_{r_1} \\ \dot{x}_{r_2} \end{bmatrix} &= \begin{bmatrix} 0 & 1 \\ -r_1 & -r_2 \end{bmatrix} \begin{bmatrix} x_{r_1} \\ x_{r_2} \end{bmatrix} + \begin{bmatrix} 0 \\ r_1 \end{bmatrix} \begin{bmatrix} u_r \end{bmatrix} \\
\begin{bmatrix} y_{r_1} \\ y_{r_2} \\ y_{r_3} \end{bmatrix} &= \begin{bmatrix} 1 & 0 \\ 0 & 1 \\ -r_1 & -r_2 \end{bmatrix} \begin{bmatrix} x_{r_1} \\ x_{r_2} \end{bmatrix} + \begin{bmatrix} 0 \\ 0 \\ r_1 \end{bmatrix} \begin{bmatrix} u_r \end{bmatrix},
\end{aligned} \tag{4.9}$$

where states are the trailing edge angle and angular velocity $x_{r_1} = \beta$, $x_{r_2} = \dot{\beta}$, input u_r is the trailing edge reference angle, and outputs y_{r_1}, y_{r_2}, y_{r_3} are the trailing edge angle and its first and second time-derivative. Constants r_1 and r_2 are set with respect to the actuator dynamics.

The assembly of the entire model can be seen in Figure 4.2. The aerodynamic model consists of a non-circulatory part and a circulatory part related to the Theodorsen function (filter $C(s)$). Aerodynamic forces are dependent on morphing trailing-edge movement coming from the actuator block and also on coupling from the elastic structural model (FEM model).

The aeroelastic wing model is rewritten in the state-space form for control design purposes. After substituting the aerodynamic forces into the structural model (4.4), the equation is rewritten in state-space form and actuator models are added. The order of state variables in the state vector is chosen as $x = \begin{bmatrix} x_0 & x_1 & \dots & x_N \end{bmatrix}^T$, where $x_i = \begin{bmatrix} \beta_i & \dot{\beta}_i & z_i & h_i & \dot{h}_i & \theta_i & \dot{\theta}_i & \phi_i & \dot{\phi}_i \end{bmatrix}^T$ are the states of the ith segment, β is the trailing edge angle (or actuator), $z_i = \begin{bmatrix} z_{h_i} & \dot{z}_{h_i} & z_{\phi_i} & \dot{z}_{\phi_i} \end{bmatrix}$ are aerodynamic lag states [47], h is the *plunge displacement*, θ is the *bending angle* and ϕ is the *torsion angle*. The overall model

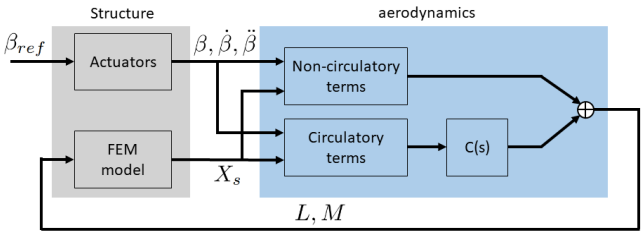

Figure 4.2: Aeroelastic model scheme

with this state variables order thus features a block tridiagonal state matrix A. The main benefit of the system matrix thus formed is in its structure where diagonal blocks can be presented as stemming from agents' autonomous dynamics and off-diagonal blocks as representing couplings among agents.

4.3 Problem Formulation

Consider an aeroelastic wing model described in Section 2. This flexible structure is decomposed into N agents modeled as Linear Time-Invariant (LTI) systems (4.10) with inherent couplings (4.11), and a decentralized control strategy is used for system damping,

$$\begin{aligned} \dot{x}_i &= A_{a_i} x_i + u_{c_i} + B_a u_i \\ y_i &= C_a x_i \\ y_{c_i} &= x_i, \end{aligned} \tag{4.10}$$

$$u_{c_i} = \sum_{j=1}^{N} \left(l_{ch_{ij}} A_{ch} + l_{cl_{ij}} A_{cl} \right) y_{c_j} \tag{4.11}$$

where $A_{a_i} \in \mathbb{R}^{n\times n}$, $B_a \in \mathbb{R}^{n\times m}$, $C_a \in \mathbb{R}^{p\times n}$; $x_i \in \mathbb{R}^n$ is the state vector of the agent i, $u_{c_i} \in \mathbb{R}^n$ is the inherent coupling of the ith agent to the remainder of the system, $u_i \in \mathbb{R}^m$ is the control input of the ith agent $y_{c_i} \in \mathbb{R}^n$ is the *coupling output* of the ith agent and $y_i \in \mathbb{R}^p$ is its *measured output*. Global inherent coupling topology is described by the *outer coupling matrices* $L_{ch} = [l_{ch_{ij}}]$ and $L_{cl} = [l_{cl_{ij}}]$, where the scalar $l_{ch_{ij}}$ ($l_{cl_{ij}}$) weights the *inner coupling matrix* A_{ch} (A_{cl}) $\in \mathbb{R}^{n\times n}$ connecting agent j and agent i

$$u_c = (L_{ch} \otimes A_{ch} + L_{cl} \otimes A_{cl}) y_c \tag{4.12}$$

The inherent couplings described in this model are usually found in flexible wing structures. The major difference from conventional cooperative multi-agent dynamics is the presence of additional terms $(L_{ch} \otimes A_{ch} + L_{cl} \otimes A_{cl})x$ interconnecting the agents. Namely, we assume that agents are *inherently* coupled, regardless of applied controls. Moreover, this coupling may differ for various network edges. This is the structure commonly found in distributed parameter systems, where high-order dynamics lead to couplings between subsystems chosen to partition the truncation of the original system.

Let us consider the dynamical model of a flexible morphing wing with a *homogenous* structure and N independent actuators. The wing root is rigidly clamped to the fuselage, and the tip of the wing is free. Then, the state matrices of agents are *identical*, except for the very last agent reflecting the boundary condition - the free wingtip. The total coupled multi-agent system S_{ab} is described by

$$\begin{aligned} \dot{x} &= (L_a \otimes A_a + L_b \otimes A_b + L_{ch} \otimes A_{ch} + L_{cl} \otimes A_{cl})x + (I_N \otimes B_a)u \\ y &= (I_N \otimes C_a)x, \end{aligned} \tag{4.13}$$

where $x = [x_1^T, ..., x_N^T]^T$, $u = [u_1^T, ..., u_N^T]^T$, $y = [y_1^T, ..., y_N^T]^T$ are the total state, input and output vectors, respectively, $L_a = \mathrm{diag}\{\mathbb{I}_{N-1}, 0\}$, $L_b = \mathrm{diag}\{\mathbb{O}_{N-1}, 1\}$.

We make the following assumption on the global interconnection topology.

Assumption 3 The outer coupling matrices are a transpose of one another, $L_{ch} = L_{cl}^T$.

$$L_{ch} = \begin{bmatrix} 0 & 1 & & \\ & \ddots & \ddots & \\ & & 0 & 1 \\ & & & 0 \end{bmatrix}; \quad L_{cl} = \begin{bmatrix} 0 & & & \\ 1 & \ddots & & \\ & \ddots & 0 & \\ & & 1 & 0 \end{bmatrix} \tag{4.14}$$

Assumption 4 The pair (A_{a_i}, B_a) is stabilizable for all A_{a_i}.

We further consider decentralized static state-feedback

$$u_i = pK_a x_i, \tag{4.15}$$

where $p > 0$ is a scalar control weight and $K_a \in \mathbb{R}^{m \times n}$ is a static state-feedback gain matrix. The overall closed-loop system is then given as

$$\begin{aligned} \dot{x} &= (L_a \otimes A_a + L_b \otimes A_b + L_{ch} \otimes A_{ch} + L_{cl} \otimes A_{cl})x + (pI_N \otimes B_a K_a)x \\ y &= (I_N \otimes C_a)x. \end{aligned} \tag{4.16}$$

4.4 Decentralized Control Design for Aeroelastic Morphing Structure

This section brings a stabilization condition for a closed-loop system (4.16), assuming global inherent coupling matrices L_{ch}, L_{cl} satisfy Assumption 3. Furthermore, we design a decentralized state-feedback (4.15) to stabilize system (4.13) to its origin.

Some technical results familiar from the literature are introduced first.

Lemma 4 [48] The LTI system $\dot{x} = Ax + Bu$ is stabilized via linear state-feedback $u = Kx$ if and only if there exists a $P > 0$ such that

$$(A + BK)^T P + P(A + BK) < 0. \tag{4.17}$$

Equivalently, if and only if there exists a $Q > 0$ such that

$$AQ + QA^T + BY + Y^T B^T < 0, \tag{4.18}$$

where $Y = KQ$.

Choosing the feedback gain K in Y as $K = -\frac{1}{2}B^T Q^{-1}$ brings an alternative stability condition

$$AQ + QA^T - BB^T < 0, \tag{4.19}$$

reducing the number of variables by one. Therefore, any $Q > 0$ satisfying (4.19), provides a stabilizing state-feedback gain $K = -\frac{1}{2}B^T Q^{-1}$. ■

Note that the last part of Lemma 4 brings a specific stabilizing control design, not only a stabilizability condition.

Lemma 5 [49] For every set of local norms on $\mathbb{R}^n$, every monotone structure norm on $\mathbb{R}^N$, and every matrix $A_G \in \mathbb{R}^{Nn \times Nn}$, $\mu(A_G) \leq \mu(A_S)$. A_G is a global matrix with the form $A_G = [A_{ij}]$ and submatrices $A_{ij} \in \mathbb{R}^{n \times n}$. $A_S \in \mathbb{R}^{N \times N}$ is associated structure matrix with the form $A_S = [a_{s_{ij}}]$, $a_{s_{ij}} = \mu(A_{ij})$.

Remark 5 Using 2-norm of a matrix and maximum singular value is equivalent, $\|A\|_2 = \overline{\sigma}(A)$, then matrix measure $\mu_2(A) = \overline{\lambda}\left(\frac{A+A^T}{2}\right)$ or $\mu_2(\hat{A}) = \overline{\lambda}(\hat{A})$ if $\hat{A}$ is a symmetric matrix. It follows that if matrix A_G is symmetric and A_S is negative definite, then A_G is also a negative definite matrix.

Lemma 6 A square matrix A is said to be *diagonally dominant* if

$$|a_{ii}| \geq |a_{ij}| \quad \text{for all} \quad i, \tag{4.20}$$

where m_{ij} denotes the entry in the ith row and jth column. A Hermitian diagonally dominant matrix M with real positive (negative) diagonal entries is positive (negative) definite.

Lemma 7 Let matrix A be a real symmetric matrix, then $\underline{\lambda}(A) > \omega_a$ if $A > \omega_a I$, where I is a unit matrix and ω_a is a real number.

Lemma 8 Let matrix A be a real matrix, then $\overline{\sigma}(A) < \omega_c$ if $A^T A < \omega_c^2 I$, or by using Schur complement $\begin{bmatrix} \omega_c I & A \\ A^T & \omega_c I \end{bmatrix} > 0$, where I is a unit matrix and ω_c is a real number.

The following theorem gives a sufficient condition for stabilizing a multi-agent system with identical agents having inherent couplings between agents (4.13).

Theorem 2 Let matrices L_{ch} and L_{cl} satisfy Assumption 3. Let there exist a $Q_a > 0$, $\omega_a > 2\omega_c$ and $\omega_b > \omega_c$ satisfying

$$\begin{aligned} A_a Q_a + Q_a A_a^T - B_a B_a^T &< 0 \\ A_b Q_a + Q_a A_b^T - B_a B_a^T &< 0 \\ \omega_a I_n + A_a Q_a + Q_a A_a^T - B_a B_a^T &< 0 \\ \omega_b I_n + A_b Q_a + Q_a A_b^T - B_a B_a^T &< 0 \\ \begin{bmatrix} -\omega_c I_n & -A_{ch}^T Q_a - Q_a A_{cl} \\ -A_{cl}^T Q_a - Q_a A_{ch} & -\omega_c I_n \end{bmatrix} &< 0. \end{aligned} \tag{4.21}$$

Then the decentralized linear state-feedback (4.15) with the feedback gain

$$K_a = -\frac{1}{2} B_a^T Q_a^{-1}, \tag{4.22}$$

and $p = 1$ stabilizes the LTI system (4.13).

Proof: Stability criterion in Lemma 4 applied to the system (4.13) requires

$$\begin{aligned} &(L_a \otimes A_a + L_b \otimes A_b + L_{ch} \otimes A_{ch} + L_{cl} \otimes A_{cl}) Q \\ &+ Q(L_a \otimes A_a + L_b \otimes A_b + L_{ch} \otimes A_{ch} + L_{cl} \otimes A_{cl})^T \\ &- (I_N \otimes B_a)(I_N \otimes B_a)^T \end{aligned} \tag{4.23}$$

to be a negative definite matrix for some positive definite $Q = Q^T \in \mathbb{R}^{n \cdot N \times n \cdot N}$. The state-feedback implied by Lemma 4 is then given by

$$K = -\frac{1}{2} (I_N \otimes B_a)^T Q^{-1}, \tag{4.24}$$

Let the matrix Q be chosen as

$$Q = I_N \otimes Q_a, \tag{4.25}$$

then the state-feedback (4.24) is in decentralized form

$$K = I_N \otimes K_a, \tag{4.26}$$

where K_a is the local state-feedback gain matrix. The choice of Q in (4.25),

renders the matrix (4.23) in the form

$$\begin{aligned}
&(L_a \otimes A_a + L_b \otimes A_b + L_{ch} \otimes A_{ch} + L_{cl} \otimes A_{cl})(I_N \otimes Q_a) \\
&+ (I_N \otimes Q_a)(L_a \otimes A_a + L_b \otimes A_b + L_{ch} \otimes A_{ch} + L_{cl} \otimes A_{cl})^T \\
&- (I_N \otimes B_a)(I_N \otimes B_a)^T \\
&= (L_a \otimes A_a Q_a + L_b \otimes A_b Q_a + L_{ch} \otimes A_{ch} Q_a + L_{cl} \otimes A_{cl} Q_a \\
&+ L_a \otimes Q_a A_a^T + L_b \otimes Q_a A_b^T + L_{ch}^T \otimes Q_a A_{ch}^T + L_{cl}^T \otimes Q_a A_{cl}^T) \\
&- I_N \otimes B_a B_a^T,
\end{aligned} \tag{4.27}$$

and Assumption 3 allows us to rewrite (4.27) as

$$\begin{aligned}
&L_a \otimes (A_a Q_a + Q_a A_a^T - B_a B_a^T) + L_b \otimes (A_b Q_a + Q_a A_b^T - B_a B_a^T) \\
&+ L_{ch} \otimes (A_{ch} Q_a + Q_a A_{cl}^T) + L_{ch}^T \otimes (A_{ch} Q_a + Q_a A_{cl}^T)^T.
\end{aligned} \tag{4.28}$$

With $A_D := (A_a Q_a + Q_a A_a^T - B_a B_a^T)$, $A_N := (A_b Q_a + Q_a A_b^T - B_a B_a^T)$ and $A_O := A_{ch} Q_a + Q_a A_{cl}^T$, the matrix (4.28) can be concisely written as a block tridiagonal matrix

$$\begin{bmatrix}
A_D & A_O & & \\
A_O^T & \ddots & \ddots & \\
 & \ddots & A_D & A_O \\
 & & A_O^T & A_N
\end{bmatrix} \in \mathbb{R}^{Nn \times Nn}. \tag{4.29}$$

By Lemma 5 and Remark 5 the sufficient condition for negative definiteness of matrix (4.29) is negative definiteness of the tridiagonal and symmetric matrix

$$\begin{bmatrix}
\mu(A_D) & \mu(A_O) & & \\
\mu(A_O^T) & \ddots & \ddots & \\
 & \ddots & \mu(A_D) & \mu(A_O) \\
 & & \mu(A_O^T) & \mu(A_N)
\end{bmatrix} \in \mathbb{R}^{N \times N}. \tag{4.30}$$

For (4.30) to be negative definite, it is sufficient that it is diagonally dominant with a negative diagonal where $|\mu(A_D)| > 2|\mu(A_O)|$ and $|\mu(A_N)| > |\mu(A_O)|$, then the diagonal elements must be negative $\mu(A_D) < 0$, $\mu(A_N) < 0$. Symmetry of A_D, A_N allows replacing their matrix measures by maximum eigenvalues (see Remark 5). Matrix measure of a generally nonsymmetric, (asymmetric), matrix A_O is replaced by the maximum singular value for which $\mu(A_O) \leq \overline{\sigma}(A_O)$ applies. Sufficient condition is then given by

$$\begin{aligned} \overline{\lambda}(A_D) < 0, \quad \underline{\lambda}(-A_D) > 2\overline{\sigma}(A_O), \\ \overline{\lambda}(A_N) < 0, \quad \underline{\lambda}(-A_N) > \overline{\sigma}(A_O). \end{aligned} \tag{4.31}$$

Substitution of minimum eigenvalues and maximum singular values according to Lemma 7 and 8 completes the proof.

Remark 6 The condition of Theorem 1 is independent of the number of agents (i.e., the size of the system). Thus, the linear state-feedback gain (4.22) stabilizes the system (4.13) for any number of agents.

Definition 1 We define system (4.13), where $A_a = A_b$ as the system S_{aa}.

Corollary 2 Let matrices L_{ch} and L_{cl} satisfy Assumption 3. Let there exist a $Q_a > 0$ and $\omega_a > 2\omega_c$ satisfying

$$\begin{aligned} A_a Q_a + Q_a A_a^T - B_a B_a^T < 0 \\ \omega_a I_n + A_a Q_a + Q_a A_a^T - B_a B_a^T < 0 \\ \begin{bmatrix} -\omega_c I_n & -A_{ch}^T Q_a - Q_a A_{cl} \\ -A_{cl}^T Q_a - Q_a A_{ch} & -\omega_c I_n \end{bmatrix} < 0. \end{aligned} \tag{4.32}$$

Then the decentralized linear state-feedback (4.15) with the feedback gain (4.22) and $p = 1$ stabilizes the LTI system S_{aa}.

Remark 7 Corollary 2 considers system S_{aa} with a simpler structure compared to that of the S_{ab}. Structure of S_{aa} describes a homogenous set of agents representing, for example, both-sides-clamped morphing wing. In other words, the boundary conditions are the same for both sides. Thus we get a simpler set of conditions, which makes it easier to find the solution.

4.5 Relaxation of the LMI Condition

This section presents an LMI relaxation procedure and control design strategy based on the developments of Section IV. Considering system S_{aa} for control design might still be infeasible for some systems. Thus we use relaxation where the inequality $\omega_a - 2\omega_c > 0$ is instead replaced by

$$\alpha\omega_a - 2\omega_c > 0, \tag{4.33}$$

where $\alpha \geq 1$. After this minor modification, the LMIs are efficiently solvable by using standard LMI tools such as MATLAB, CVX, MOSEK, etc.

With respect to this simplification and relaxation, the solution must be verified by substituting the resulting Q_a into the matrix (4.29), and checking if it is indeed negative definite. Then the resulting controller also stabilizes the system S_{ab} with a nonhomogenous set of agents.

The following algorithm based on considerations from Remark 7 offers a feasible method for finding stabilizing decentralized state feedback for the system S_{ab}. The proposed control design is presented on a numerical model of a flexible morphing wing from Section 2. The structure has 20 nodes, and the order of the system is 240. By an appropriate arrangement of state variables in the system model, we obtain a dynamical system in the form of the S_{ab} with the single-agent dynamics given by system matrices $A_a(A_b) \in \mathbb{R}^{6\times 6}$ and the inner coupling matrices $A_{ch}(A_{cl}) = \mathbb{R}^{6\times 6}$. Each agent has one control

input. The topology of the underlying inherent interconnections between the agents is described by the matrix $L_{ch} \in \mathbb{R}^{N\times N}$ and $L_{cl} \in \mathbb{R}^{N\times N}$. The following algorithm describes the decentralized system control design based on Corollary 2.

Algorithm 2

1. Set $\alpha = 1$
2. Solve LMIs

$$\begin{aligned} A_a Q_a + Q_a A_a^T - B_a B_a^T &< 0 \\ \omega_a I_n + A_a Q_a + Q_a A_a^T - B_a B_a^T &< 0 \\ \begin{bmatrix} -\omega_c I_n & A_{ch}^T Q_a + Q_a A_{cl} \\ A_{cl}^T Q_a + Q_a A_{ch} & -\omega_c I_n \end{bmatrix} &< 0 \\ -Q_a &< 0 \\ 2\omega_c - \alpha\omega_a &< 0 \end{aligned}$$

3. If LMIs are not feasible, decrease α and go to 2)
4. Substitute Q_a into (4.29)
5. Check if the matrix (4.29) is negative definite
6. Compute the local state feedback gain K_a (4.22)

4.6 Simulation Case Study

This section brings the numerical experiment using the aeroelastic model from Section 2. In the controller synthesis and system analysis below, an aeroelastic model with 240 states meaning 20 agents of order 12, is used. Parameters of the model are chosen to correspond to a 2m aeroelastic wing with 1st structural mode having the frequency of 3.28Hz and 2nd structural mode 20.61Hz. The wing parameters were chosen concerning natural frequencies from experimental modal analysis [50] to get closer to the real wing behavior. The flutter speed of our model was determined based on the system's pole movement in the complex plane concerning airspeed. All system poles were in the left half complex plane until the airspeed 22m/s, where the system became unstable. Therefore the airspeed of 22m/s is also a flutter (or critical) speed.

After applying Algorithm 2 to the aeroelastic morphing wing model, we obtain the stabilizing state feedback gain matrix K_a. The resulting closed-loop system response is compared in the frequency domain with the undamped morphing wing in Figure 4.3. For all Bode plots, the input is the first node vertical disturbance, and the output is the 20th node vertical displacement. The magnitude Bode plot of both systems shows closed-loop damping. Despite of system stabilization and its significant damping, the first resonant frequency and DC gain was shifted. From a practical point of view, this controller feature is not desirable.

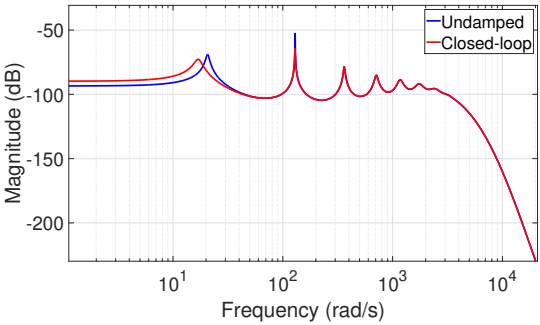

Figure 4.3: Bode magnitude plots of the undamped flexible morphing wing and flexible morphing wing with the decentralized state-feedback.

Remark 8 The resonant frequency and DC gain shift do not occur for a homogenous set of agents, i.e., when $A_a = A_b$. For this case, Algorithm 2 is suitable in its current form.

Frequency and DC gain shift elimination could be achieved by adding high-pass (HP) filters into the control design. Let us consider the effects of first-order HP filter, HP_i, modeled as a Linear Time-Invariant (LTI) systems with matrices

$$A_{HP} = \begin{bmatrix} -500 \end{bmatrix}; B_{HP} = \begin{bmatrix} -490 \end{bmatrix}; C_{HP} = \begin{bmatrix} 1 \end{bmatrix}; D_{HP} = \begin{bmatrix} 1 \end{bmatrix} \tag{4.34}$$

having the cutoff frequency of 10 rad/s. We define a new system S_{ab}^{HP} where each input i to the system S_{ab} is filtered with a HP filter HP_i. Then the Algorithm 2 is executed for system S_{ab}^{HP}.

It is necessary to connect HP_i behind the local state feedback pK_a for closing the feedback and obtaining the closed-loop system. In other words, the control law consists of decentralized state feedback and HP filters.

Comparison between frequency and time responses is given in Figure

4.4. The closed-loop system is stable and damped, while resonant frequencies and DC gain remain very similar to the original values of an open-loop/(undamped) system. Moreover, the scalar control weight p can be used for final controller tuning, setting the aggressiveness of the control law by a single constant. Figures 4.4 also show possible differences between controllers with different values $p_1 < p_2$.

The controller with p_2 is more aggressive and it is also able to damp the system more effectively. However, the control input (Figure 4.4c) with p_2 has a larger magnitude. The controller must be tuned with respect to the control input and its saturation.

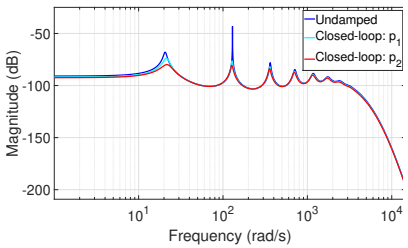

(a) Bode magnitude plots.

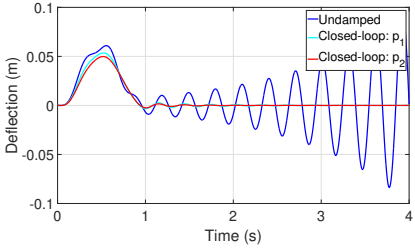

(b) Responses to 1-cos gust - last node.

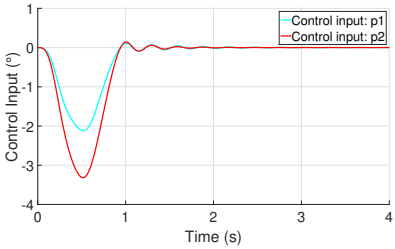

(c) Control inputs - last node.

Figure 4.4: Undamped flexible morphing wing and flexible morphing wing with the decentralized state-feedback, scalar control weights p_1, p_2, and HP filters.

The robustness of the control law with respect to parameter uncertainties and model imperfections is demonstrated below. Model parameters vary typically due to dynamic pressure changes within a defined flight envelope, and imperfections of the model can be attributed to identification inaccuracies of aerodynamic and mass parameters of the airframe. For our system example, robustness is demonstrated in the frequency domain by showing the regions containing magnitude Bode plots of the open-loop/undamped and closed-loop systems for different values of parameters. Robustness analysis is done for the controller with control weight p_2. Figure 4.5 shows both systems with varying aerodynamic parameters corresponding to International Civil Aviation Organization (ICAO) Standard Atmosphere from altitude 0m to 10000m. The variation of a selected mass parameter, namely the total mass from 4kg to 8kg, is in Figure 4.6. The red curve corresponds to the design model parameters, which is the middle of both intervals (5000m, 6kg).

Figures 4.5 and 4.6 show the ability of the proposed controller to satisfactorily dampen the wing even under significant uncertainties in the model parameters.

In Figure 4.5 where the altitude was changed, the frequency response shift is evident in the Magnitude direction. This magnitude change is significantly smaller for a closed-loop system, which is stable for the entire range and all magnitude peaks are well-damped. The variation of the mass parameter from Figure 4.6 shows frequency responses shifting in the frequency axis. Also, in this case, the closed-loop system is stable for the whole range, and magnitude peaks are reduced effectively. Therefore the damping function of the controller is robust with respect to significant model parameter changes.

The performance of the control law was also investigated in the terms of flutter stability. The aeroelastic wing model has critical flutter speed 22m/s. We reached an improvement of 41% by using decentralized controller with scalar control weight p_2 from previous example. It means, the critical flutter

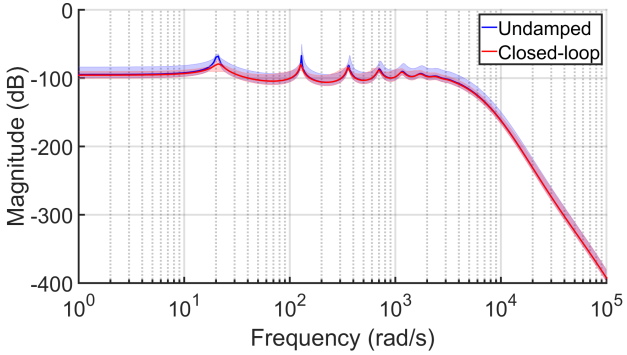

Figure 4.5: Bode magnitude plots of undamped systems and closed-loop systems with various pressure and temperature parameters (transparent colored areas), solid lines correspond to design model parameters.

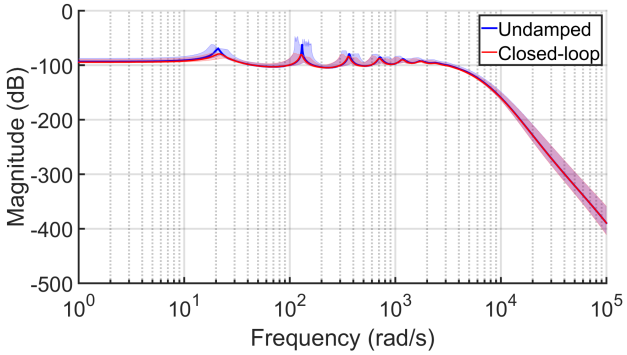

Figure 4.6: Bode magnitude plots of undamped systems and closed-loop systems with various mass parameter (colored areas), solid lines correspond to design model parameters.

speed with the controller is 31m/s.

Increased damping of aeroelastic modes is also responsible for gust re-

sponse improvement. In the time simulation shown in the Figure 4.7 we can see a "1-cosine" discrete gust [51] response of undamped and closed-loop systems. For the sake of clarity, only ten agents' responses are depicted. The time simulation was performed with a free-stream velocity of 22.5m/s where the (uncontrolled) wing becomes unstable. In contrast to undamped system the capability for gust load attenuation with decentralized controller is clear. Figure 4.8 also shows the root bending moment reduction of the wing with the control system and corresponding control action.

The wing deflection naturally increases with increasing distance from the wing root. The same applies to control input which is the largest for the wing tip (Figure 4.8). This gradual increase of the trailing-edge angle of our decentralized controller is apparent from Figure 4.9c

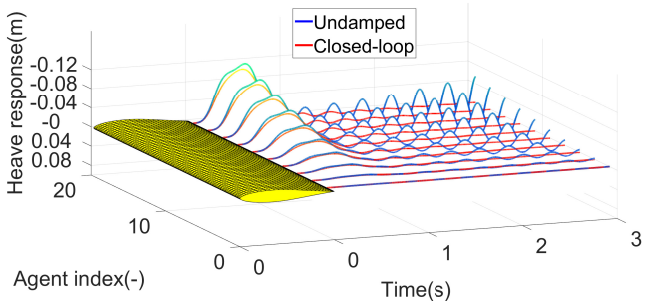

Figure 4.7: 1-cosine discrete gust time response of undamped and closed-loop systems.

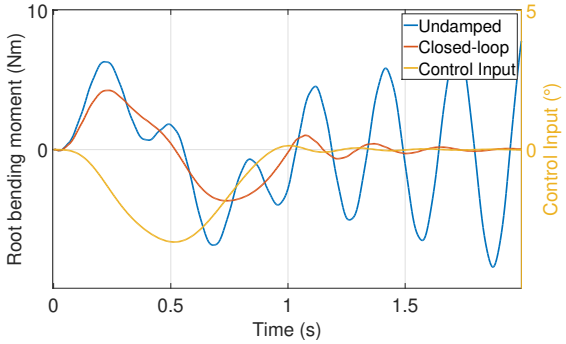

Figure 4.8: Root bending moment and control input : 1-cosine discrete gust.

In the following example, we compare the achieved result with the standard LQR design. The LQ controller is centralized, and it assumes all states available. In this case, the airspeed was 16 m/s (under flutter speed) to focus on the vibration control only. The resulting graphs are depicted in Figure 4.9.

By tuning the weighting matrices Q and R we obtained a similar time response as we have for the decentralized controller. However, the control input is completely different. A decentralized controller distributes the control action across all agents (all wing segments in the wingspan). Therefore the maximum trailing-edge deflection for all wing actuators is under 2°. Despite the similar time responses, the LQR uses the largest control to the last node (over 3°), and other control actions to other nodes are almost negligible. This property is more significant if the Q and R are just scaled unit matrices with the same diagonal elements. In the example in Figure 4.9, weights corresponding to the last node are 10^5 smaller than others. If these weights are more similar, then the damping is lower, and the control action of the last node is greater.

The aggressiveness of a decentralized controller can be simply modified

by one parameter. LQR tuning of course, provides more freedom in tuning through many elements in matrices Q, R. However, the controller tuning for systems with hundreds of states or more could be challenging. LQR design or other control method design for systems with hundreds of agents could be computationally demanding or even intractable. Our control method design is scalable and thus suitable even for such large systems.

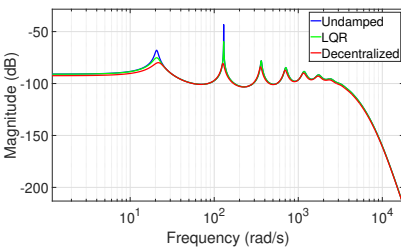

(a) Bode magnitude plots.

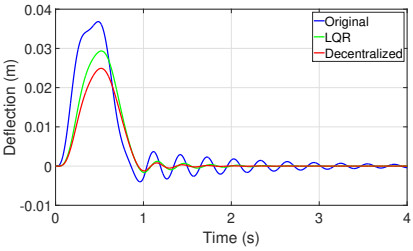

(b) Responses to 1-cos gust - last node.

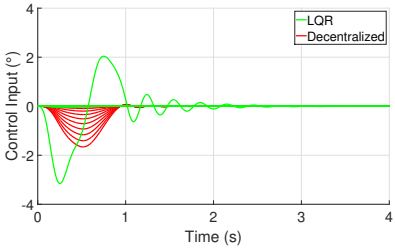

(c) Control inputs.

Figure 4.9: Comparison of decentralized controller wit LQR.

4.7 Conclusion

In this paper, we present a novel decentralized control design technique for an aeroelastic morphing wing. This technique uses a multi-agent interpretation of the system to take advantage of the system structure and its recurring local

dynamics. The result is a decentralized control law designed based on agent dynamics and inherent couplings. It is these inherent couplings that make it impossible to use standard cooperative control methods straightforwardly. In addition, the controller synthesis is feasible even for a large number of agents, and thus the presented technique is suitable even for large complex systems. The control design procedure is demonstrated on a numerical example of a flexible morphing wing. We highlight some possible closed-loop issues, their solution, and also the controller robustness to parameter uncertainties. Finally, we compare our control design approach with LQR design, where our controller tuning simplicity was evident.

References

[1] Y. Ouyang, Y. Gu, X. Kou, Z. Yang, Active flutter suppression of wing with morphing flap, Aerospace Science and Technology 110. doi:10.1016/j.ast.2020.106457.

[2] S. Guo, Z. Jing, H. Li, W. Lei, Y. He, Gust response and body freedom flutter of a flying-wing aircraft with a passive gust alleviation device, Aerospace Science and Technology 70 (2017) 277–285. doi:https://doi.org/10.1016/j.ast.2017.08.008.

[3] T. A. Weisshaar, Morphing aircraft systems: Historical perspectives and future challenges, Journal of Aircraft 50 (2013) 337–353. doi:10.2514/1.C031456.

[4] S. Barbarino, O. Bilgen, R. M. Ajaj, M. I. Friswell, D. J. Inman, A review of morphing aircraft, Journal of Intelligent Material Systems and Structures 22 (9) (2011) 823–877. doi:10.1177/1045389X11414084.

[5] J. Urnes, N. Nguyen, C. Ippolito, K. Trinh, E. Ting, A mission adaptive variable camber flap control system to optimize high lift and cruise lift to drag ratios of future n+3 transport aircraft, in: 51st AIAA Aerospace Sciences Meeting, 2013. doi:10.2514/6.2013-214.

[6] N. Nguyen, Elastically shaped future air vehicle concept, in: NASA Innovation Fund Award 2010, NASA, 2010.

[7] N. Nguyen, N. Cramer, K. Hashemi, M. Drew, J. Xiong, T. Mundt, M. Mor, E. Livne, Progress on gust load alleviation wind tunnel experiment and aeroservoelastic model validation for a flexible wing with variable camber continuous trailing edge flap system, in: AIAA SciTech Forum, AIAA, 2020. doi:10.2514/6.2020-0214.

[8] Z. Wang, X. Yang, B. Li, Sma-actuated morphing wing with varying spanwise curvature and sweptangle, in: 2019 IEEE International Conference on Robotics and Biomimetics (ROBIO), IEEE, 2019, pp. 1615–1620. doi:10.1109/ROBIO49542.2019.8961458.

[9] N. Nguyen, S. Lebofsky, E. Ting, U. Kaul, D. Chaparro, J. Urnes, Development of variable camber continuous trailing edge flap for performance adaptive aeroelastic wing, in: SAE AeroTech Congress & Exhibition, NASA, 2015. doi:10.4271/2015-01-2565.

[10] Y. Zhang, W. Ge, Z. Zhang, X. Mo, Y. Zhang, Design of compliant mechanism-based variable camber morphing wing with nonlinear large deformation, International Journal of Advanced Robotic Systems 16. doi:10.1177/1729881419886740.

[11] G. Molinari (Ed.), Multidisciplinary Optimization of Morphing Wings with Distributed Compliance and Smart Actuation, Doctoral Thesis, ETH Zurich, 2016.

[12] B. Jenett, S. Calisch, D. Cellucci, N. Cramer, N. Gershenfeld, S. Swei, K. Cheung, Digital morphing wing: Active wing shaping concept using composite lattice-based cellular structures, Soft Robotics 4. doi:10.1089/soro.2016.0032.

[13] D. Keidel, J. Sodja, N. Werter, R. D. Breuker, P. Ermanni, Development and testing of an unconventional morphing wing concept with variable chord and camber, in: 26th International Conference on Adaptive Structures and Technologies, TU Delft, 2015, pp. 1–12.

[14] D. A. Burdette, G. K. Kenway, J. Martins, Performance evaluation of a morphing trailing edge using multipoint aerostructural design optimization, in: 57th AIAA/ASCE/AHS/ASC Structures, Structural Dynamics, and Materials Conference, AIAA, 2016, pp. 1–15. doi:10.2514/6.2016-0159.

[15] L. Gamble, D. Inman, Bioinspired pitch control using a piezoelectric horizontal tail for rudderless uavs, in: SPIE Smart Structures and Materials + Nondestructive Evaluation and Health Monitoring, 2018, Denver, Colorado, United States, 2018. doi:10.1117/12.2287471.

[16] Z. Hui, Y. Zhang, G. Chen, Aerodynamic performance investigation on a morphing unmanned aerial vehicle with bio-inspired discrete wing structures, Aerospace Science and Technology 95. doi:10.1016/j.ast.2019.105419.

[17] H. Zhou, A. R. Plummer, D. J. Cleaver, Distributed actuation and control of a tensegrity based morphing wing, IEEE/ASME Transactions on Mechatronicsdoi:10.1109/TMECH.2021.3058074.

[18] F. Auteri, A. Savino, A. Zanotti, G. Gibertini, D. Zagaglia, Y. B. Tekap, M. Braza, Experimental evaluation of the aerodynamic performance of a

large-scale high-lift morphing wing, Aerospace Science and Technology 124. doi:10.1016/j.ast.2022.107515.

[19] A. Mushfiqul, M. Hromčík, Structural load alleviation using distributed delay shaper: Application to flexible aircraft, Control Engineering Practice 89 (2019) 130–142. doi:10.1016/j.conengprac.2019.05.005.

[20] J. Wijnja, S. R, R. Breuker, Aeroelastic analysis of a large airborne wind turbine, Journal of Guidance, Control, and Dynamics 41 (11) (2018) 130–142. doi:10.2514/1.G001663.

[21] Y. LIU, C. XIE, Aeroservoelastic stability analysis for flexible aircraft based on a nonlinear coupled dynamic model, Chinese Journal of Aeronautics 31 (12) (2018) 2185–2198. doi:https://doi.org/10.1016/j.cja.2018.08.019.

[22] J. Lunze, Networked Control of Multi-Agent Systems, Bookmundo Direct, 2019.

[23] R. Olfati-Saber, J. A. Fax, R. M. Murray, Consensus and cooperation in networked multi-agent systems, Proceedings of the IEEE 95 (1) (2007) 215–233. doi:10.1109/JPROC.2006.887293.

[24] Z. Li, Z. Duan, G. Chen, Consensus of multiagent systems and synchronization of complex networks: A unified viewpoint, IEEE Transactions on Circuits and Systems 57-I (2010) 213–224. doi:10.1109/TCSI.2009.2023937.

[25] H. Zhang, F. L. Lewis, A. Das, Optimal design for synchronization of cooperative systems: state-feedback, observer and output feedback, IEEE Transactions on Automatic Control 56 (8) (2011) 1948–1952. doi:10.1109/TAC.2011.2139510.

[26] Y. Hong, X. Wang, Z. Jiang, Multi-agent coordination with general linear models: A distributed output regulation approach, in: IEEE ICCA 2010, IEEE, 2010, pp. 137–142. doi:10.1109/ICCA.2010.5524157.

[27] K. H. Movric, F. L. Lewis, Cooperative optimal control for multi-agent systems on directed graph topologies, IEEE Transactions on Automatic Control 59 (3) (2014) 769–774. doi:10.1109/TAC.2013.2275670.

[28] W. W. Zhang, Root locus approach to a distributed parameter vibrating system with both bending and torsion motions, International Journal of Mechanical Sciences 37 (6) (1995) 585–600. doi:10.1016/0020-7403(94)00001-Z.

[29] H. Liu, X. Wang, Aeroservoelastic design of piezo-composite wings for gust load alleviation, Journal of Fluids and Structures 88 (2019) 83–99. doi:10.1016/j.jfluidstructs.2019.04.010.

[30] M. Krommer, H. Irschik, M. Zellhofer, Design of actuator networks for dynamic displacement tracking of beams, Mechanics of Advanced Materials and Structures 15 (3-4) (2008) 235–249. doi:10.1080/15376490801907764.

[31] H. Irschik, M. Nader, Actuator placement in static bending of smart beams utilizing mohr's analogy, Engineering Structures 31 (8) (2009) 1698–1706. doi:10.1016/j.engstruct.2009.02.026.

[32] N. Chopra, M. Spong, Passivity-based control of multi-agent systems, Advances in robot control 34 (2006) 107–134. doi:10.1007/978-3-540-37347-6_6.

[33] D. Halim, S. O. R. Moheimani, Spatial resonant control of flexible structures-application to a piezoelectric laminate beam, IEEE Trans-

actions on Control Systems Technology 9 (1) (2001) 37–53. doi:10.1109/87.896744.

[34] R. D'Andrea, A linear matrix inequality approach to decentralized control of distributed parameter systems, in: Proceedings of the 1998 American Control Conference, IEEE, 1998, pp. 1350–1354. doi:10.1109/ACC.1998.707015.

[35] L. Jankowski, B. Poplawski, G. Mikulowski, A. Mroz, Decentralized semi-active damping of free structural vibrations by means of structural nodes with an on/off ability to transmit moments, Mechanical Systems and Signal Processing 100 (2018) 926–939. doi:10.1016/j.ymssp.2017.08.012.

[36] Y. Li, G. Yang, Adaptive fuzzy decentralized control for a class of large-scale nonlinear systems with actuator faults and unknown dead zones, IEEE Transactions on Systems, Man, and Cybernetics: Systems 47 (5) (2017) 729–740. doi:10.1109/TSMC.2016.2521824.

[37] B. Labibi, B. Lohmann, A. K. Sedigh, P. J. Maralani, Decentralized stabilization of large-scale systems via state-feedback and using descriptor systems, IEEE Transactions on Systems, Man, and Cybernetics - Part A: Systems and Humans 33 (6) (2003) 771–776. doi:10.1109/TSMCA.2003.818463.

[38] N. Luo, R. J, M. De la Sen, Decentralized active control of a class of uncertain cable-stayed flexible structures, International Journal of Control 75 (4) (2002) 285–296. doi:10.1080/00207170110110559.

[39] P. Hušek, F. Svoboda, M. Hromčík, Z. Šika, Low-complexity decentralized active damping of one-dimensional structures, Shock and Vibration (2018) 1–9doi:10.1155/2018/6421604.

[40] J. Xiang, Y. Li, D. J. Hill, Cooperative output regulation of multi-agent systems coupled by dynamic edges 47 (3) (2014) 1813–1818. doi:10.3182/20140824-6-ZA-1003.02164.

[41] T. Theodorsen, General theory of aerodynamic instability and the mechanism of flutter, in: Rep. NACA-TR-496, NASA Center for AeroSpace Information, Langley Research Center, Hampton, Virginia, 1949.

[42] L. Ünlüsoy, Y. Yaman, Aeroelastic behaviour of uav wings due to morphing, Aircraft Engineering and Aerospace Technology 89 (1) (2017) 30–38. doi:10.1108/AEAT-12-2014-0217.

[43] D. Durmuş (Ed.), Aeroelastic analysis of variable-span morphing wing, M. Sc. Thesis, Istanbul Technical University, Istanbul, 2020. doi:10.13140/RG.2.2.35176.90889.

[44] J. Zhang, A. Shaw, C. Wang, H. Gu, M. Amoozgar, M. Friswell, B. Woods, Aeroelastic model and analysis of an active camber morphing wing, Aerospace Science and Technology 111. doi:10.1016/j.ast.2021.106534.

[45] J. Wright, J. Cooper, Introduction to Aircraft Aeroelasticity and Loads: Second Edition, 2nd Edition, Wiley, 2015.

[46] F. Svoboda, M. Hromčík, Finite element method based modeling of a flexible wing structure, in: 21st International Conference on Process Control, Strbske Pleso, Slovakia, IEEE, 2017. doi:10.1109/PC.2017.7976217.

[47] R. T. Jones, Operational treatment of the nonuniform-lift theory in airplane dynamics, NACA TN 667.

[48] S. Boyd, L. E. Ghaoui, E. Feron, V. Balakrishnan, Linear matrix inequalities in system and control theory, SIAM studies in applied mathematics 15 (1994) 30–38.

[49] G. Russo, M. di Bernardo, E. D. Sontag, A contraction approach to the hierarchical analysis and design of networked systems, IEEE Transactions on Automatic Control 58 (5) (2013) 1328–1331. doi:10.1109/TAC.2012.2223355.

[50] J. Simsiriwong, R. Sullivan, Experimental vibration analysis of a composite uav wing, Mechanics of Advanced Materials and Structures - MECH ADV MATER STRUCT 19 (2012) 196–206. doi:10.1080/15376494.2011.572248.

[51] W. Tian, Y. Gu, H. Liu, X. Wang, Z. Yang, Y. Li, P. Li, Nonlinear aeroservoelastic analysis of a supersonic aircraft with control fin freeplay by component mode synthesis technique, Journal of Sound and Vibration 493 (2021) 115835. doi:10.1016/j.jsv.2020.115835.

List of Author's Publications

Publications in Journals with Impact Factor

[1] F. Svoboda, K. Hengster-Movric, M. Hromčík, Z. Šika, Decentralized active damping control for aeroelastic morphing wing, Aerospace Science and Technology 139 (2023) 108415, [Journal Impact Factor: 5.6]. doi:https://doi.org/10.1016/j.ast.2023.108415.

[2] F. Svoboda, K. Hengster-Movric, M. Hromčík, Decentralized control for large scale systems with inherently coupled subsystems, Journal of Vibration and Control 28 (23-24) (2022) 3931–3938, [Journal Impact Factor: 2.8]. doi:10.1177/10775463211034953.

[3] P. Hušek, F. Svoboda, M. Hromčík, Z. Šika, Low-complexity decentralized active damping of one-dimensional structures, Shock and Vibration 2018 (2018) 1–9, [Journal Impact Factor: 1.6]. doi:10.1155/2018/6421604.

International Conference Papers

[1] F. Svoboda, M. Hromcik, Active flutter suppression by means of fixed-order h control: results for the benchmark active control technology (bact) wing, in: Proceedings of 18th European Control Conference (ECC), 2019, pp. 119–124. doi:10.23919/ECC.2019.8795733.

[2] F. Svoboda, M. Hromčík, K. Hengster-Movric, Distributed state feedback control for aeroelastic morphing wing flutter supression, in: Proceedings of 26th Mediterranean Conference on Control and Automation (MED), 2018, pp. 575–580. doi:10.1109/MED.2018.8442815.

[3] Z. Šika, M. Hromčík, J. Volech, F. Svoboda, J. Zavřel, J. Králíček, Decentralized and distributed mimo h-infinity robust control of vibration suppression of planar structures, in: Proceedings of ISMA2018 International Conference on Noise and Vibration Engineering, 2018, pp. 309–323.

[4] F. Svoboda, M. Hromčík, Distributed control for a morphing wing with a macro fiber composite actuator, in: Proceedings of the SMS EUROPE 2018, Italy, International Conference, 2018.

[5] J. Volech, Z. Šika, F. Svoboda, M. Hromčík, J. Králíček, Control of vibration suppression of planar structures using actuation by clusters of piezopatches, in: Proceedings of the SMS EUROPE 2018, Italy, 2018.

[6] F. Svoboda, M. Hromčík, Z. Šika, Adaptive control design for the aeroelastic wing, in: Proceedings of 23rd International Conference on Process Control (PC), 2021, pp. 225–228. doi:10.1109/PC52310.2021.9447451.

[7] F. Svoboda, M. Hromčík, Construction of the smooth morphing trailing edge demonstrator, in: Proceedings of 22nd International Conference on Process Control (PC19), 2019, pp. 136–139. doi:10.1109/PC.2019.8815050.

[8] F. Svoboda, M. Hromčík, Finite element method based modeling of a flexible wing structure, in: Proceedings of 21st International Conference on Process Control (PC), 2017, pp. 222–227. doi:10.1109/PC.2017.7976217.

[9] P. Beneš, Z. Šika, M. Hromčík, F. Svoboda, A. Balon, Shavo control of a morphing wing, in: Computational Mechanics 2019, 2019.

[10] J. Volech, Z. Šika, M. Hromčík, F. Svoboda, J. Zavřel, Vibration suppression and shape change of thin plate by clusters of actuators, in: Computational Mechanics 2019, 2019.

[11] J. Králíček, Z. Šika, J. Volech, F. Svoboda, M. Hromčík, Vibration control of cantilever beam using collocated piezoelectric sensor/actuator pair, in: Bulletin of Applied Mechanics, Vol. 13, 2017, pp. 1–6.

[12] F. Svoboda, M. Hromčík, Adaptive control design for the aeroelastic wing, in: "What's New in Aerospace?". Praha, 2016.

[13] P. Kočárník, J. Roháč, M. Hromčík, M. Strob, F. Svoboda, Elektron i, in: "What's New in Aerospace?". Praha, 2016.

[14] A. Kratochvíl, F. Svoboda, T. Sommer, S. Slavík, Design for active flutter suppresion and model verification, in: Proceedings of International Scientific Congress Innovations in Engineering 2016. Sofia: Scientific-technical union of mechanical engineering, 2016, pp. 47–50.

[15] A. Kratochvíl, F. Svoboda, T. Sommer, S. Slavík, Design for active flutter suppresion and model verification, in: TRANS MOTAUTO WORLD, no. 4, 2016, pp. 7–10.